Delft University of Technology
Faculty of Electrical Engineering, Mathematics and Computer Science
Delft Institute of Applied Mathematics

Mathematical modeling of angiogenesis and contraction occuring during wound healing in soft tissues

A thesis submitted to the
Delft Institute of Applied Mathematics
in partial fulfillment of the requirements

for the degree

MASTER OF SCIENCE
in
APPLIED MATHEMATICS

by

Olmer van Rijn

Delft, the Netherlands
August 2010

TU Delft

MSc THESIS APPLIED MATHEMATICS

"Mathematical modeling of angiogenesis and contraction occuring during wound healing in soft tissues"

Olmer van Rijn

Delft University of Technology

Daily supervisor

Dr.ir. F.J. Vermolen

Responsible professor

Prof.dr.ir. C. Vuik

Other thesis committee members

Dr.ir. M. Keijzer

August 2010

Delft, the Netherlands

Contents

Chapter 1

Introduction

For every animal's survival it is vital for its body to be able to repair injured parts. When injured the body responds with a series of events, beginning with containing the damage and working towards recovery. The biological model described in [1] and summarized below describes the various stages of the wound healing process.

In medicine the cutaneous wound healing process is generally divided into three partly overlapping stages. These stages mainly consist of (1) inflammation, (2) granulation tissue formation and (3) wound closure. In the inflammation stage the body attempts to contain the damage. The inflammatory process tries to either destroy, dilute or wall off the injurious agent. Along with removing the cause of the injury it starts off the healing process, [1].

In the second stage granulation tissue is formed in the wound. Fibroblasts invade the wound area and contract the surrounding tissue (extracellular matrix) to ensure that new small blood vessels, capillaries, can be formed (angiogenesis). As new blood capillaries are formed, oxygen and nutrients can once again be transported to the wound side.

Finally when the tissue is provided with enough oxygen and nutrients the process of wound closure starts. Cells in the epidermis, which mainly consist of keratinocytes, start regenerating the upperlayer of the wound. Usually the skin can not be replaced fully and some marks are left where the wound was located, like scars.

The second and third stage of wound healing do not take place at the same location in the wound. The former is located in the dermis, the latter is limited to the epidermis. The epidermis and the dermis consist of different type of cells and are separated by a so-called basal membrane, see also Figure 1.1.

In this thesis we first present a selection of the currently available mathematical models that seek to describe the biological processes of wound healing as well as possible. The healing process is very complex and many factors contribute to it, therefore simplifications have to be made. In Chapter 2 we give a detailed description to which mathematical wound healing models this has led so far.

The main topics in this thesis are combining two models for angiogenesis and coupling models for the different stages of wound healing. Currently models exist for the different stages separately, but only scarcely have there been attempts to couple the models. This is vital as the various stages of wound healing overlap and hence influence each other.

Such coupled models could give more insights on how the process of wound healing works. These insights might lead to treatments that reduce healing time, e.g. the use of certain hormones to speed up the healing process. Also scars and other deformations due to incomplete healing might be prevented or reduced.

For several models simulations have been done to give more insight on how these models

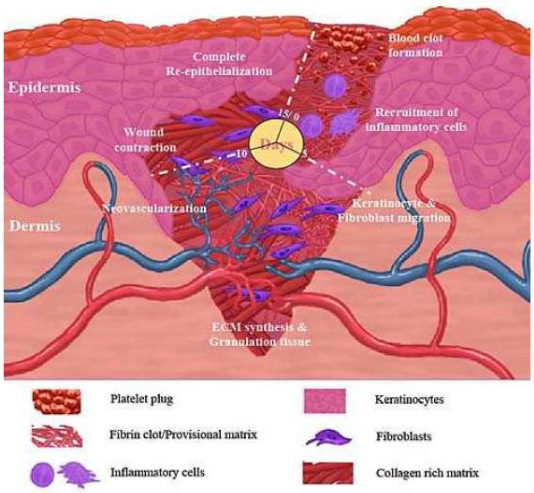

Figure 1.1: A schematic of the events during wound healing. The dermis and epidermis are illustrated. The picture was taken with permission from http://www.bioscience.org/2006/v11/af/1843/figures.htm

behave. Also the dependence of the models on certain parameters is investigated. Finally recommendations are made for future research in the topic of mathematically describing wound healing.

Chapter 2

Currently available mathematical models

The mathematical model for the proliferative stage of wound healing is usually separated in three distinct parts representing three stages of wound healing. These three stages are wound contraction, angiogenesis and wound closure. Note that the inflammation stage mentioned in Section 1 is not taken into account. This is due to the fact that inflammation only contains the damage and only after the inflammation stage is finished the real healing process starts.

In this chapter we present some of the currently available models on the above mentioned wound healing stages. In Section 2.1 we first present three models on wound contraction. Each model is an extension of the previous as it incorporates an extra aspect of wound contraction. Next in Section 2.2 two models on angiogenesis are presented. The two models take a very different approach on how to model the growth of new blood vessels in the wound. For the third stage, wound closure, two models are presented in section 2.3. In Section 2.4 a study that attempts to combine models of the three stages is briefly discussed. In all the models that we deal with, we consider a bounded simply connected domain $\Omega \subset \mathbb{R}^2$. The boundary is denoted by $\partial\Omega$.

2.1 Wound contraction models

During the wound contraction stage fibroblasts (connective tissue cells) invade the wound site and contract the extracellular matrix (ECM). The contraction decreases the area of contact between the wound and its surroundings, thus reducing the chance of contamination and infection. Furthermore this process is vital in assuring that new blood vessels can be formed in the wound during angiogenesis, since the fibroblasts invading the wound form the tissue in which the new capillaries can grow. The wound contraction stage is limited to the dermis, but the contraction of the ECM also effects the tissue in the epidermis.

All the wound contraction models are based on the linear viscoelastic equations, i.e.

$$-\nabla \cdot \sigma = \mathbf{f}_{\text{ext}}. \tag{2.1}$$

Here $\sigma = \sigma_{\text{ecm}} + \sigma_{\text{cell}}$, the stresstensor, accounts for the ECM related stress, σ_{ecm}, and the cell stress, σ_{cell}. Furthermore $\mathbf{f}_{\text{ext}}$ represents the external forces acting on the tissue.

In all the below discussed models the ECM related stress tensor σ_{ecm} is given as

$$\sigma_{\text{ecm}} = \mu_1 \frac{\partial \epsilon}{\partial t} + \mu_2 \frac{\partial \theta}{\partial t}\mathbf{I} + \frac{E}{1+\nu}\left(\epsilon + \frac{\nu}{1-2\nu}\theta\mathbf{I}\right). \tag{2.2}$$

Here the first two terms on the right hand side respresent the viscous effects and the last term the elastic effects. If we let $\mathbf{u} = \mathbf{u}(\mathbf{x}, t)$ denote the displacement of the ECM, then the strain tensor ϵ and the dilation θ in equation (2.2) are respectively given by

$$\epsilon = \frac{1}{2}\left(\nabla\mathbf{u} + (\nabla\mathbf{u})^T\right) \tag{2.3}$$

and

$$\theta = \nabla \cdot \mathbf{u}. \tag{2.4}$$

Furthermore, in (2.2), $\mathbf{I}$ denotes the identity tensor and μ_1, μ_2, E and ν respectively represent the dynamic and kinematic viscosity, Young's modulus and Poisson's ratio.

Also the external forces acting on the tissue, $\mathbf{f}_{\text{ext}}$, are modelled similarly in all three models, i.e.

$$\mathbf{f}_{\text{ext}} = -s\rho\mathbf{u}. \tag{2.5}$$

Here $\rho = \rho(\mathbf{x}, t)$ denotes the ECM density and s is the tethering elasticity coefficient.

At time $t = 0$ it is assumed that there is no displacement of the ECM, i.e. $\mathbf{u}(\mathbf{x}, 0) = \mathbf{0}$. Also we assume that $\mathbf{u}$ vanishes at the boundary far away from the wound, i.e. $\mathbf{u}(\mathbf{x}, t) = \mathbf{0}$ for $\mathbf{x} \in \partial\Omega$. This can be justified by taking the computational domain Ω sufficiently large, so that the boundary effects can be ignored.

2.1.1 The model of Tranquillo

In this section we present the wound contraction model due to Tranquillo, [2]. It is the most simple formulation of the three models as it only covers (in combination with the viscoelastic equations) the change of the fibroblast concentration and the ECM density in time.

Fibroblasts are motile cells and thus are subject to, besides being diffused by passive convection caused by the ECM displacement, diffusion. Furthermore, the fibroblast concentration is affected by fibroblast production, which is assumed to follow a logistic growth pattern. All together this gives us the partial differential equation (PDE) for the fibroblast concentration $u_{\text{fib}} = u_{\text{fib}}(\mathbf{x}, t)$ as

$$\frac{\partial u_{\text{fib}}}{\partial t} + \nabla \cdot \left(\frac{\partial \mathbf{u}}{\partial t} u_{\text{fib}} - D_{\text{fib}} \nabla u_{\text{fib}}\right) = \lambda_{\text{fib}} u_{\text{fib}} \left(u^0_{\text{fib}} - u_{\text{fib}}\right). \tag{2.6}$$

Here D_{fib} denotes the diffusion coefficient, λ_{fib} the fibroblast production rate and u^0_{fib} the equilibrium fibroblast concentration. In equation (2.6) the second term on the left hand side accounts for both passive and active convection. The term on the right hand side represents the fibroblast production.

For the ECM density $\rho = \rho(\mathbf{x}, t)$ we find a similar PDE, but since the ECM is nonmotile and consists of very long molecular chains, the diffusion term is negligible. Also the ECM production is assumed to depend on the fibroblast concentration. This leads to

$$\frac{\partial \rho}{\partial t} + \nabla \cdot \left(\frac{\partial \mathbf{u}}{\partial t} \rho\right) = \lambda_{\text{ecm}} u_{\text{fib}} \left(\rho^0 - \rho\right), \tag{2.7}$$

where λ_{ecm} is the ECM production rate and ρ^0 denotes the ECM equilibrium density.

The cell traction term, σ_{cell}, used in the model due to Murray and Tranquillo depends on both the ECM density and the fibroblast concentration. The higher the ECM density and the fibroblast concentration the larger the stress is on the ECM. The cell traction term is thus, in this model, given by

$$\sigma_{cell} = \frac{\tau \rho u_{\text{fib}}}{1 + \lambda u^2_{\text{fib}}} \mathbf{I}, \tag{2.8}$$

where λ quantifies how the cell traction depends on the fibroblast concentration and τ is a proportionality constant.

For the fibroblast concentration we impose a no flux boundary condition, this is justified by taking the computation domain Ω sufficiently large. Since $\mathbf{u} = \mathbf{0}$ on the boundary, we have $\frac{\partial \mathbf{u}}{\partial t} = 0$ on $\partial\Omega$, and hence no boundary condition has to be imposed on $\partial\Omega$ for ρ. Note that if we do not assume zero displacement at the boundary we have to impose a boundary condition for ρ. Furthermore, at time $t = 0$ we assume both quantities to be zero inside the wound, i.e.

$$u_{\text{fib}}(\mathbf{x}, 0) = 0, \rho(\mathbf{x}, 0) = 0$$

for $\mathbf{x} \in \Omega_w$, and to be at their equilibrium outside the wound, i.e.

$$u_{\text{fib}}(\mathbf{x}, 0) = u^0_{\text{fib}}, \rho(\mathbf{x}, 0) = \rho^0$$

for $\mathbf{x} \in \Omega_u$. Here Ω_w denotes the wounded and $\Omega_u = \Omega \setminus \Omega_w$ the undamaged tissue.

2.1.2 The model of Olsen et al

The model for wound contraction proposed by Olsen et al. in [3] differs from Tranquillo's model in two ways. In the first place, it deals with the presence of myofibroblasts. Myofibroblasts are a kind of weak muscle cells. They are nonmotile cells that differentiate from fibroblasts and transmit and amplify the traction forces generated by the fibroblasts, [8]. Secondly, the model incorporates the effects of a growth factor that triggers wound contraction.

In addition to new PDEs for both the myofibroblast and growth factor concentration some differences are found in the other governing equations. The equation concerning the fibroblast concentration u_{fib} becomes

$$\frac{\partial u_{\text{fib}}}{\partial t} + \nabla \cdot \left(\frac{\partial \mathbf{u}}{\partial t} u_{\text{fib}} - D_{\text{fib}} \nabla u_{\text{fib}} + \frac{a_{\text{fib}}}{(b_{\text{fib}} + c_{\text{ecm}})^2} u_{\text{fib}} \nabla c_{\text{ecm}} \right) =$$
$$\left(\lambda_{\text{fib}} + \frac{\lambda^0_{\text{fib}} c_{\text{ecm}}}{C_{1/2} + c_{\text{ecm}}} \right) u_{\text{fib}} \left(1 - \frac{u_{\text{fib}}}{K} \right) - \frac{k_1 c_{\text{ecm}}}{C_k + c_{\text{ecm}}} u_{\text{fib}} + k_2 u_{\text{myo}} - d_{\text{fib}} u_{\text{fib}}, \tag{2.9}$$

where c_{ecm} and u_{myo} respectively denote the growth factor and myofibroblast concentration. The cell death rate is denoted by d_{fib}, the myofibroblast to fibroblast differentiation rate by k_2 and the fibroblast to myofibroblast differentiation rate by k_1. Furthermore λ^0_{fib}, $C_{1/2}$ and C_k are known constants that monitor the growth factor's influence on the contraction process and K is a parameter that regulates the equilibrium concentration.

If we compare equation (2.9) with equation (2.6) we see that there is an extra convective term, the fourth term on the left hand side. This term accounts for cell movement due to chemotaxis. Chemotaxis is the phenomenon in which, in this case, fibroblasts are attracted by a chemical, in this case the growth factor. The production term, first on the right hand side, now also incorporates growth factor stimulated proliferation. The other three terms on the right hand side respectively account for differentiation to and from myofibroblasts and cell death.

The PDE for the myofibroblast concentration u_{myo} is similar to equation (2.9). But since myofibroblast are nonmotile cells, they will only move due to passive convection. The myofibroblast concentration thus solves

$$\frac{\partial u_{\text{myo}}}{\partial t} + \nabla \cdot \left(\frac{\partial \mathbf{u}}{\partial t} u_{\text{myo}} \right) = \varepsilon_{\text{myo}} \left(\lambda_{\text{fib}} + \frac{\lambda^0_{\text{fib}} c_{\text{ecm}}}{C_{1/2} + c_{\text{ecm}}} \right) u_{\text{myo}} \left(1 - \frac{u_{\text{myo}}}{K} \right)$$
$$+ \frac{k_1 c_{\text{ecm}}}{C_k + c_{\text{ecm}}} u_{\text{fib}} - k_2 u_{\text{myo}} - d_{\text{myo}} u_{\text{myo}}, \tag{2.10}$$

where ε_{ecm} is a proportionality constant and d_{myo} and u^0_{myo} denote the myofibroblasts death rate and the myofibroblast equilibrium concentration respectively.

Both fibroblasts and myofibroblasts contribute to the production of the ECM, furthermore the production is chemically enhanced by the growth factor, [8]. The PDE for the ECM density ρ then is given by

$$\frac{\partial \rho}{\partial t} + \nabla \cdot \left(\frac{\partial \mathbf{u}}{\partial t} \rho \right) = \left(\lambda_\rho + \frac{\lambda^0_\rho c_{\text{ecm}}}{C_\rho + c_{\text{ecm}}} \right) \frac{u_{\text{fib}} + \eta_b u_{\text{myo}}}{R^2_\rho + \rho^2} - d_\rho (u_{\text{fib}} + \eta_d u_{\text{myo}}) \rho, \tag{2.11}$$

where λ_ρ and d_ρ are the ECM production and death rate respectively. Furthermore λ^0_ρ and C_ρ are known constants that monitor the growth factor's influence on the contraction process. R_ρ is a parameter that quantifies how the ECM production rate depends on the ECM density itself and η_b and η_d are proportionality constants.

The dynamics of the growth factor concentration c_{ecm} are mainly determined by the fibroblasts and myofibroblasts as they produce the growth factor. Also the growth factor is motile, so it is subject to active convection. This leads to the following PDE for the growth factor concentration

$$\frac{\partial c_{\text{ecm}}}{\partial t} + \nabla \cdot \left(\frac{\partial \mathbf{u}}{\partial t} c_{\text{ecm}} - D_c \nabla c_{\text{ecm}} \right) = \frac{k_c (u_{\text{fib}} + \zeta u_{\text{myo}}) c_{\text{ecm}}}{\Gamma + c_{\text{ecm}}} - d_c c_{\text{ecm}}. \tag{2.12}$$

Here the second and third term on the left hand side account for passive and active convection. The terms on the right hand side account for growth factor production and growth factor decay respectively. Furthermore D_c is the growth factor diffusion coefficient, k_c denotes the growth factor production rate and d_c the decay rate. Also Γ is a parameter that quantifies how the growth factor production rate depends on the growth factor concentration itself and ζ is a proportionality constant.

Since the myofibroblasts transmit and amplify the traction forces generated by the fibroblasts this is also visible in the cell traction term σ_{cell}. For the model due to Olsen et al. this term is given by

$$\sigma_{\text{cell}} = \frac{\tau u_{\text{fib}} \left(1 + \xi u_{\text{myo}}\right) \rho}{R^2_\tau + \rho^2} \mathbf{I}, \tag{2.13}$$

where ξ is a proportionality constant and R_τ quantifies how the cell traction depends on the ECM density.

The initial and boundary conditions for the fibroblast concentration and the ECM density remain the same as in the model due to Tranquillo. For the myofibroblast and growth factor concentration the following initial conditions are imposed

$$u_{\text{myo}}(\mathbf{x}, 0) = 0, c_{\text{ecm}}(\mathbf{x}, 0) = c^0_{\text{ecm}}$$

for $\mathbf{x} \in \Omega_w$ and

$$u_{\text{myo}}(\mathbf{x}, 0) = 0, c_{\text{ecm}}(\mathbf{x}, 0) = 0$$

for $\mathbf{x} \in \Omega_u$. Here c^0_{ecm} denotes the growth factor equilibrium concentration. Furthermore the growth factor concentration satisfy a no flux boundary condition on all boundaries. For the myofibroblast concentration we can apply the same reasoning as for the ECM density ρ and hence no boundary conditions have to be imposed.

2.1.3 The model of Javierre

In [11] an extension of the model due to Olsen et al. is presented. Javierre et al. propose the mechanical stress to act as a factor that effects the differentiation from fibroblasts to myofibroblasts. They introduce an estimation of the mechanical stimulus that depends on the dilation $\theta = \nabla \cdot \mathbf{u}$ as

$$p_{\text{cell}}(\theta) = \frac{K_{\text{act}} p_{\max}}{K_{\text{act}}\theta_1 - p_{\max}} (\theta_1 - \theta)\, \chi_{[\theta_1,\theta^*]}(\theta) + \frac{K_{\text{act}} p_{\max}}{K_{\text{act}}\theta_2 - p_{\max}} (\theta_2 - \theta)\, \chi_{[\theta_2,\theta^*]}(\theta) + K_{\text{pas}}\theta. \quad (2.14)$$

Here χ denotes the indicator function, i.e.

$$\chi_I(\theta) = \begin{cases} 1, & \text{if } \theta \in I, \\ 0, & \text{else.} \end{cases}$$

and the first two terms on the right hand side account for the contractile stress generated internally by the myosin machinery and transmitted through the actin bundles, [11]. The third term on the right hand side establishes the contractile stress supported by the passive resistance of the cell. See also Figure 2.1 for a plot of $p_{\text{cell}}(\theta)$.

Furthermore, in equation (2.14), the compression and traction strain limits are respectively denoted by θ_1 and θ_2, $p_{\max}$ respresents the maximal contractile force exerted by the actomyosin machinery and $K_{\max}$ and K_{pas} the volumetric stiffness moduli of the active and passive components of the cell. Also the parameter θ^* can be computed from K_{act} and $p_{\max}$ as $\theta^* = \frac{p_{\max}}{K_{\text{act}}}$, [11].

To incorporate the effects of the mechanical stimulus on the fibroblast to myofibroblast differentiation an extra factor is found before the differentiation term (the second term on the right hand side) in equation (2.9). The fibroblast to myofibroblast differentiation term changes to

$$\frac{p_{\text{cell}}(\theta)}{\tau_d + p_{\text{cell}}(\theta)} \frac{k_1 c_{\text{ecm}}}{C_k + c_{\text{ecm}}} u_{\text{fib}}, \quad (2.15)$$

where τ_d is a parameter that quantifies how the differentiation rate depends on the mechanical stimulus. Note that this term is also present in the PDE for the myofibroblast concentration and that thus the second term on the right hand side of equation (2.10) also changes to the above.

The mechanical stimulus also effects the the cell stresses and thus the cell traction term σ_{cell}. In [11] it is assumed that σ_{cell} depends linearly on $p_{\text{cell}}(\theta)$ and thus that

$$\sigma_{\text{cell}} = p_{\text{cell}}(\theta) \frac{u_{\text{fib}}\,(1 + \xi u_{\text{myo}})\,\rho}{R_\tau^2 + \rho^2} \mathbf{I}. \quad (2.16)$$

In order to give more insight in the process of wound contraction we did some simulations with the model due to Javierre et al. The simulations have been done using numerical techniques described in Chapter 6. As a computational domain we use the unit square, i.e. $\Omega = \{\mathbf{x} = (x, y) |\ 0 \le x, y \le 1\}$, and the initial wound is given by $\Omega_w = \left\{\mathbf{x} |\ |\mathbf{x}| \le \frac{1}{2}\right\}$. The results are given in Figures 2.2 to 2.4, where we show the solution two days after injury. The computations have been done using parameter values taken from [11].

In Figure 2.2 we show the fibroblast and myofibroblast concentration two days after injury. The myofibroblast concentration is highly concentrated around the wound edge, whereas the fibroblast have invaded the wound. If we compare Figure 2.4 with Figure 2.2 we see that the ECM displacement is largest at places of high myofibroblast concentration. Here the effect of the myofibroblasts, as they transmit and amplify the traction forces generated by the fibroblasts, can clearly be seen.

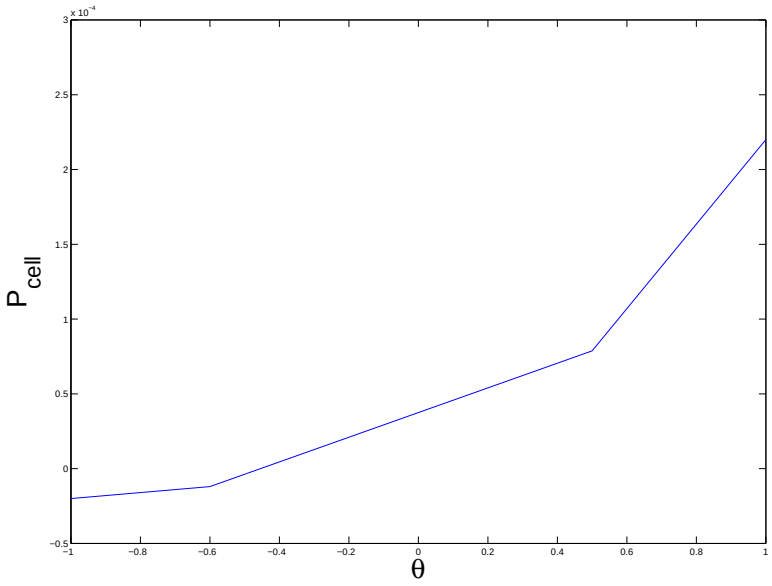

Figure 2.1: The mechanical stimulus p_{cell} as a function of the dilation θ, computed with values from [11].

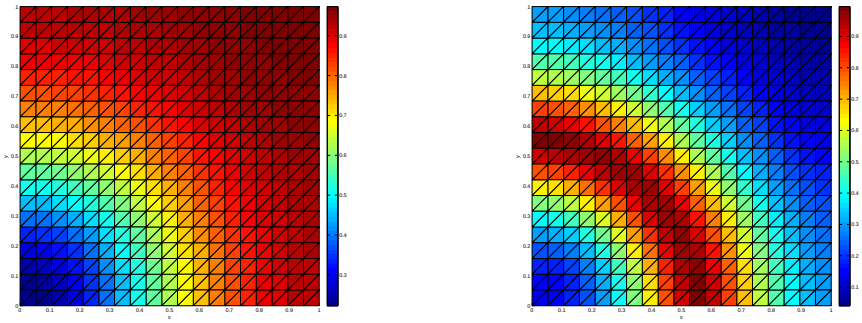

Figure 2.2: Normalized fibroblast (left) and myofibroblast (right) concentration two days after injury.

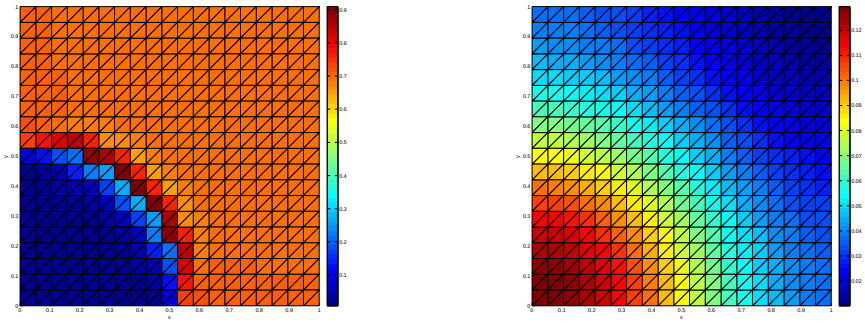

Figure 2.3: Normalized ECM density (left) and growth factor concentration (right) two days after injury.

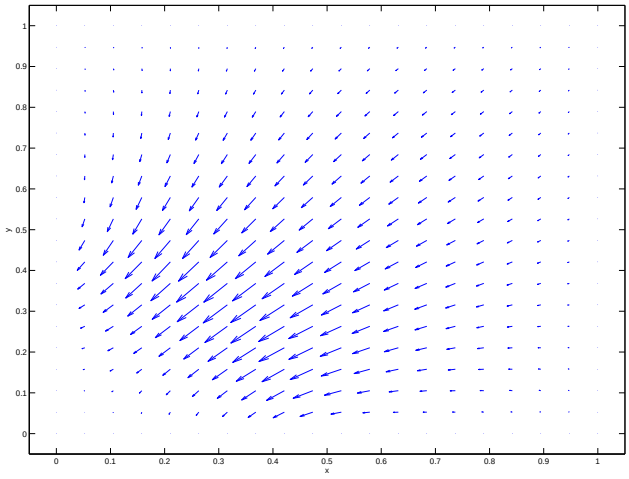

Figure 2.4: Displacement of the ECM two days after injury.

Figure 2.3 shows the ECM density and the growth factor concentration two days after injury. We see that the ECM density is slightly elevated at the wound edge, which is to be expected since the wound is healing there. Furthermore the growth factor concentration has spread throughout the computational domain, but is still concentrated inside the wound.

The normalized solutions in time at $\mathbf{x} = \mathbf{0}$, furthest in the wound, are shown in Figure 2.5. This gives an indication of the development of the solutions in time. We see that the fibroblast concentration rises towards it equilibrium, whereas the myofibroblast concentration first rises and then falls again. This is due to the fact that, as the wound heals, the myofibroblasts differentiate back to fibroblasts again and eventually will disappear completely. Also the growth factor concentration eventually goes to zero as the wound is healed. The ECM density slowly rises in time and will eventually reach its equilibrium, allthough it can take some time before the ECM is completely restored.

2.2 Angiogenesis models

Angiogenesis is the wound healing stage that succeeds and partly overlaps wound contraction. The fibroblast invasion during wound contraction gives the wound a stable structure for new capillaries to grow in. These new capillaries can then provide the wound with oxygen and nutrients needed for healing. This process, which takes place in the dermis, is modelled in two very different ways.

2.2.1 The model of Maggelakis

The model due to Maggelakis, proposed in [4], assumes a positive relation between the lack of oxygen in the wound and the growth of new capillaries. The shortage of oxygen activates macrophages in the wound area, which in their turn start the production of a growth factor that stimulates capillary regeneration, [8]. In return, the growth of new capillaries reduces the shortage of oxygen due to transport. The flow chart of this system can be seen in Figure 2.6.

If we let u_{oxy}, c_{md} and u_{cap} respectively denote the oxygen concentration, the macrophage derived growth factor (MDGF) concentration and the capillary density, the model due to Magge-

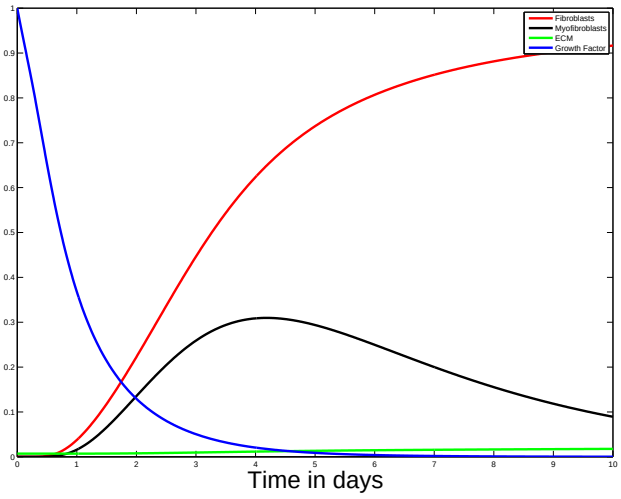

Figure 2.5: Normalized solutions furthest in the wound, at $\mathbf{x} = \mathbf{0}$, in time.

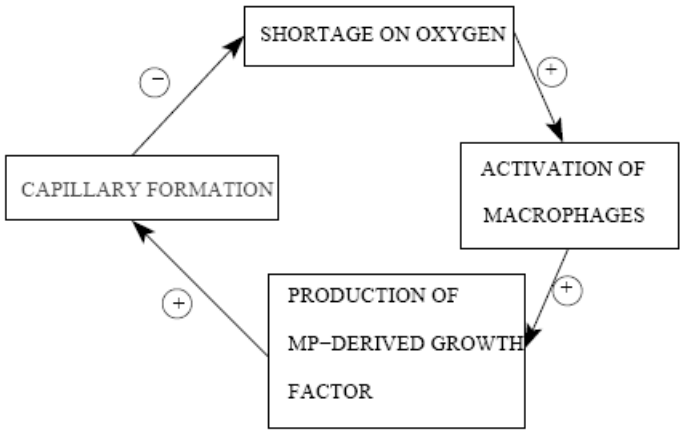

Figure 2.6: A schematic of the negative feedback mechanism for the model for angiogenesis due to Maggelakis. The +/- signs denote that the increase has a positive/negative effect on the quantity. This image was taken with permission from [8].

lakis follows as

$$\frac{\partial u_{\text{oxy}}}{\partial t} = D_{\text{oxy}}\Delta u_{\text{oxy}} - \lambda_{\text{oxy}} u_{\text{oxy}} + \lambda_{13} u_{\text{cap}}, \tag{2.17}$$

$$\frac{\partial c_{\text{md}}}{\partial t} = D_{\text{md}}\Delta c_{\text{md}} - \lambda_{\text{md}} c_{\text{md}} + \lambda_{21} Q(u_{\text{oxy}}), \tag{2.18}$$

$$\frac{\partial u_{\text{cap}}}{\partial t} = D_{\text{cap}}\Delta u_{\text{cap}} + \lambda_{\text{cap}} c_{\text{md}} u_{\text{cap}} \left(1 - \frac{u_{\text{cap}}}{u^0_{\text{cap}}}\right). \tag{2.19}$$

Here the D_i are the diffusion coefficients, whereas the terms $\lambda_{\text{oxy}} u_{\text{oxy}}$ and $\lambda_{\text{md}} c_{\text{md}}$ respectively represent the oxygen consumption and the decay of the growth factor. The MDGF production rate Q depends on the oxygen concentration in the following way

$$Q(u_{\text{oxy}}) = \begin{cases} 0, & \text{if } \mathbf{x} \in \Omega_u, \\ 0, & \text{if } u_{\text{oxy}} \geq u_\theta, \\ 1 - \frac{u_{\text{oxy}}}{u_\theta}, & \text{if } u_{\text{oxy}} < u_\theta, \end{cases}$$

where u_θ is a given threshold value for the MDGF production. So the production of MDGF drops linearly to zero when the oxygen concentration is below the threshold value u_θ and rising.

The last term in equation (2.19) accounts for the formation of new capillaries, where u^0_{cap} is the equilibrium capillary density. The capillary growth is assumed to be logistic and is triggered by the presence of the macrophage derived growth factor. The term $\lambda_{13} u_{\text{cap}}$ in (2.17) captures the transport of oxygen towards the wound, which is larger if there are more capillaries.

The initial conditions are given by

$$u_{\text{oxy}}(\mathbf{x}, 0) = \begin{cases} 0 & \text{if } \mathbf{x} \in \Omega_w, \\ u^0_{\text{oxy}} & \text{if } \mathbf{x} \in \Omega_u, \end{cases}$$

$$c_{\text{md}}(\mathbf{x}, 0) = 0,$$

$$u_{\text{cap}}(\mathbf{x}, 0) = \begin{cases} 0 & \text{if } \mathbf{x} \in \Omega_w, \\ u^0_{\text{cap}} & \text{if } \mathbf{x} \in \Omega_u. \end{cases}$$

Here u^0_{oxy} and u^0_{cap} denote the equilibrium solutions for the oxygen concentration and the capillary density respectively. So initially the wound itself is void of oxygen, capillaries and MDGF, whereas in the healthy tissue enough oxygen is available and the capillary network is intact. For all three variables we impose no flux boundary conditions. This is reasonable due to symmetry and when taking the computational domain Ω large.

2.2.2 The model of Gaffney et al.

The model proposed in [5] by Gaffney et al. takes a completely different approach to model angiogenesis. It models the relation between the capillary tip concentration and the endothelial cell density, which is a building block for new blood capillaries, [8]. It does not take into account the relation between shortage of oxygen and growth of new capillaries.

The model due to Gaffney et al. tries to capture the process where endothelial cells migrate out of blood vessels facing the wound. As they migrate they form tubes that extend from the parent vessel, [8]. At the tips of these tubes cells proliferate to form new capillaries that extend into the wound area. Tips branch and join and thus form a new network of capillaries, from which the process is repeated until the capillary network is completely restored.

If we let $u_{\text{tip}} = u_{\text{tip}}(\mathbf{x}, t)$ and $u_{\text{end}} = u_{\text{end}}(\mathbf{x}, t)$ be the capillary tip concentration and the endothelial cell density respectively, then the partial differential equations of this model read

$$\frac{\partial u_{\text{tip}}}{\partial t} = \nabla \cdot \{D_1 \nabla u_{\text{tip}} + D_2 u_{\text{tip}} \nabla u_{\text{end}}\} + f(u_{\text{tip}}, u_{\text{end}}) \tag{2.20}$$

$$\frac{\partial u_{\text{end}}}{\partial t} = \lambda_1 \nabla \cdot \{D_1 \nabla u_{\text{tip}} + D_2 u_{\text{tip}} \nabla u_{\text{end}}\} + g(u_{\text{tip}}, u_{\text{end}}). \tag{2.21}$$

The first term on the right hand side in both equations denotes transport as well as an additional migration towards a decreasing blood vessel density, [8]. The two functions f and g both depend on the capillary tip concentration and the endothelial cell density. They represent production and decay of u_{tip} and u_{end} respectively.

For the capillary tip concentration growth is only due to tip branching, the splitting of tips into new tips. Decay can either be caused by two tips meeting at one point or a tip meeting a capillary. Since the probability that a tip is located at a certain point is proportional to u_{tip}, the growth term is also proportional to u_{tip}. Decay due to two tips meeting then is proportional to u_{tip}^2, whereas decay casued by a tip meeting a capillary is proportional to $u_{\text{tip}} u_{\text{end}}$. All this combined gives us the function f as

$$f(u_{\text{tip}}, u_{\text{end}}) = \lambda_2 u_{\text{tip}} - \lambda_3 u_{\text{tip}}^2 - \lambda_4 u_{\text{tip}} u_{\text{end}}. \tag{2.22}$$

The function $g(u_{\text{tip}}, u_{\text{end}})$ can be split into four separate terms. The first denoting proliferation due to logistic growth of the endothelial cell density, [8]. The second term accounts for extra growth due to the presence of tips, which are build from endothelial cells. The third and fourth term are taken together and represent growth due to two tips joining or one tip merging with a capillary (compare to the last two terms in equation (2.22)). The whole function g is then given by

$$\begin{aligned} g(u_{\text{tip}}, u_{\text{end}}) =& \lambda_6 a u_{\text{end}}(u_{\text{end}}^0 - u_{\text{end}}) + \lambda_6 \chi u_{\text{tip}} u_{\text{end}}(u_{\text{end}}^1 - u_{\text{end}}) \\ &+ \lambda_5(\lambda_3 u_{\text{tip}}^2 + \lambda_4 u_{\text{tip}} u_{\text{end}}). \end{aligned} \tag{2.23}$$

At the boundary of the computational domain Ω it is assumed that no transport takes place of both capillary tips and endothelial cells, so they both satisfy a no flux boundary condition. This is reasonable due to symmetry and when taking Ω large. Furthermore it is assumed that inside the wound area, $\mathbf{x} \in \Omega_w$, there are no capillary tips and endothelial cells initially present. Outside the wound area, the endothelial cell concentration is at its equilibrium, u_{end}^0, due to a undamaged capillary network. The capillary tip concentration is everywhere zero, except for a small strip facing the wound area.

2.3 Wound closure models

The final stage of the healing process is closure of the wound. When the wounded area has been sufficiently supplied with oxygen and nutrients, cells in the epidermis start dividing and so regenerate the damaged skin as good as possible. This process is triggered by numerous growth factors, but in the following two models it is assumed that only one generic growth factor influences wound closure, [8]. Note that this process takes place in the epidermis, unlike wound contraction and angiogenesis. This should be taken into account if one wants to couple a wound closure model with a model of wound contraction or angiogenensis. This because these two processes only influence wound closure at the boundary between the dermis and the epidermis, the basal membrane.

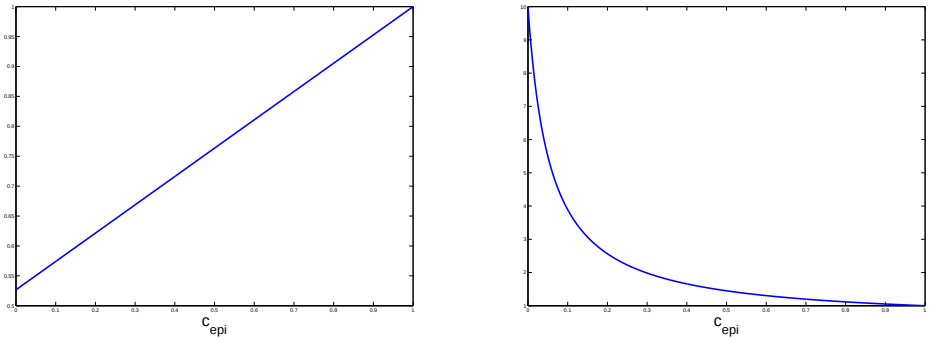

Figure 2.7: The function $s(c_{\text{epi}})$ for an activator (left) and an inhibitor (right).

2.3.1 The model of Sherratt and Murray

If the density of epidermal cells is low, the production of the epidermal cell derived growth factor is high. And under the influence of the growth factor the production of epidermal cells increases. Those are the basics for the model due to Sherratt and Murray proposed in [6]. As the wound heals, the production of epidermal cells decreases to a point where the proliferation rate is in balance with the decay rate, [8].

If we let u_{epi} denote the epidermal cell density then its balance is given by

$$\frac{\partial u_{\text{epi}}}{\partial t} = D_{\text{epi}}\Delta u_{\text{epi}} + s(c_{\text{epi}})u_{\text{epi}}\left[2 - \frac{u_{\text{epi}}}{u_{\text{epi}}^{\text{eq}}}\right] - \lambda_{\text{epi}}u_{\text{epi}}, \tag{2.24}$$

where the terms on the right hand side account for diffusive transport, proliferation and cell death respectively. The growth factor concentration is denoted by u_5 and s is a nonlinear function of this concentration describing the mitotic rate.

Sherratt and Murray consider two different types of growth factors, activators and inhibitors. The function $s(c_{\text{epi}})$ is different in both cases and reads

$$s(c_{\text{epi}}) = \frac{2c_m(h-\beta)c_{\text{epi}}}{c_m^2 + c_{\text{epi}}^2} + \beta \tag{2.25}$$

for the activator and

$$s(c_{\text{epi}}) = \frac{(h-1)c_{\text{epi}} + h}{2(h-1)c_{\text{epi}} + 1} \tag{2.26}$$

for the inhibitor, here h and c_m are known constants and

$$\beta = \frac{1 + c_m^2 - 2hc_m}{(1-c_m)^2}$$

The function $s(c_{\text{epi}})$ is plotted in Figure 2.7 for $h = 10$ and $c_m = 40$.

The growth factor concentration behaves similarly to equation (2.24) and thus for u_5 we obtain

$$\frac{\partial c_{\text{epi}}}{\partial t} = D_{\text{egf}}\Delta c_{\text{epi}} + f(u_{\text{epi}}) - \lambda_{\text{egf}}c_{\text{epi}}. \tag{2.27}$$

Here the function f is a nonlinear function of u_{epi}, which is also different in the activator and inhibitor case. For the activator case it is given by

$$f(u_{\text{epi}}) = \frac{u_{\text{epi}}(1+\alpha^2)}{u_{\text{epi}}^2 + \alpha^2}, \tag{2.28}$$

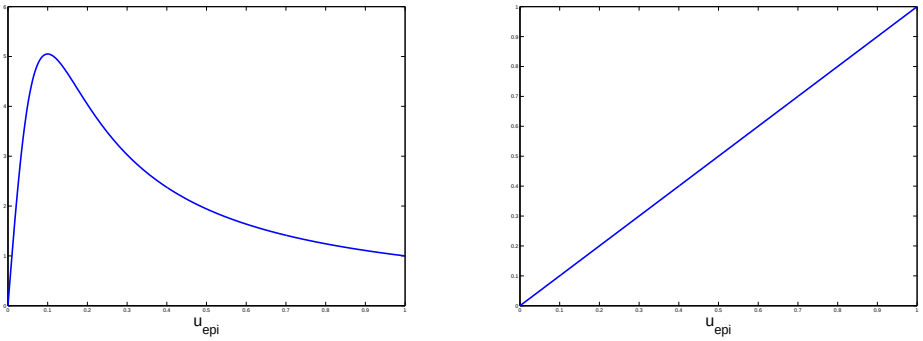

Figure 2.8: The function $f(u_{\text{epi}})$ for an activator (left) and an inhibitor (right).

where α is a constant, and for the inhibitor it is given by

$$f(u_{\text{epi}}) = u_{\text{epi}}. \tag{2.29}$$

The function $f(u_{\text{epi}})$ is plotted in Figure 2.8 for $\alpha = 0.1$.

For both the epidermal cell density and the growth factor concentration the initial value is zero inside the wound and both are at their equilibrium outside the wound, i.e.

$$u_{\text{epi}}(\mathbf{x}, 0) = \begin{cases} 0, & \text{for } \mathbf{x} \in \Omega_w \\ u_{\text{epi}}^{\text{eq}}, & \text{for } \mathbf{x} \in \Omega_u \end{cases}$$

$$c_{\text{epi}}(\mathbf{x}, 0) = \begin{cases} 0, & \text{for } \mathbf{x} \in \Omega_w \\ c_{\text{epi}}^{\text{eq}}, & \text{for } \mathbf{x} \in \Omega_u. \end{cases}$$

Furthermore it is assumed that there is no transport of both epidermal cells and growth factor over the boundaries of the computational domain. Thus a no-flux boundary condition is induced on both u_{epi} and c_{epi}.

2.3.2 The model of Adam

The model due to Adam, proposed in [7], takes a somewhat different approach as it only considers the dynamics of the growth factor concentration. Then based on the presence of the growth factor the healing process is described, [8].

Firstly, the computational domain Ω is split up in three subdomains $\Omega_1(t)$, $\Omega_2(t)$ and $\Omega_3(t)$. They denote the wound area, the active layer and the outer (healthy) tissue respectively and are functions of time since the wound is healing.

The presence of growth factor is influenced by diffusive transport, decay and production. If we denote its concentration by c, the partial differential equation for the growth factor is given by

$$\frac{\partial c}{\partial t} = \nabla \cdot (D \nabla c) - \lambda c + P \chi_{\Omega_2}(\mathbf{x}), \tag{2.30}$$

where D, λ and P are the diffusion coefficient, decay factor and production rate respectively. Furthermore

$$\chi_{\Omega_2}(\mathbf{x}) = \begin{cases} 1, & \text{for } \mathbf{x} \in \Omega_2(t) \\ 0, & \text{for } \mathbf{x} \in \Omega_1(t) \cup \Omega_3(t), \end{cases} \tag{2.31}$$

the indicator function of $\Omega_2(t)$. On the boundary $\partial\Omega$ we assume no transport of the growth factor and thus a no-flux boundary condition is imposed. Initially the growth factor is assumed to be absent in the entire computational domain, [8].

If we denote the interface between $\Omega_1(t)$ and $\Omega_2(t)$ by $W(t)$,

$$W(t) = \bar{\Omega}_1(t) \cap \bar{\Omega}_2(t), \tag{2.32}$$

then healing at a certain location on $W(t)$ implies that the inward normal component of the velocity, v_ν, is positive, [8]. The model due to Adam, see [7], says that this is so when the growth factor concentration exceeds a certain value, i.e. $v_\nu \neq 0$ if and only if $c(\mathbf{x}, t) > \hat{c}$, for $\mathbf{x}$ on the interface $W(t)$.

Furthermore it is assumed that the healing rate is proportional to the local curvature κ of the wound. Then the velocity component in the outward (from $\Omega_1(t)$) normal direction is given by

$$v_\nu = -(\alpha + \beta\kappa) w(c(t, \mathbf{x}) - \hat{c}). \tag{2.33}$$

Here α and β are positive constants, prohibiting growth of the wound if $\kappa \geq 0$, and $w(s)$ falls within the family of Heaviside functions.

So to know if the wound is healing at a certain location along the interface $W(t)$, one needs to know the growth factor concentration there. To know the rate of healing, one must look at the curvature of the wound.

2.4 Coupled model

The models described in the previous sections all account for a single stage in the wound healing process. In fact these stages (partially) overlap each other in the healing process and thus are also influenced by one another. Furthermore where wound contraction and angiogenesis are dermal processes, wound closure occurs in the epidermis.

In [9] an attempt is made to combine models of the three stages to get more insight in the wound healing process, such as geometry influences. The model due to Murray and Tranquillo, see Section 2.1.1, is used for wound contraction. For angiogenesis and wound closure the model due to Maggelakis, see Section 2.2.1, and Sherratt and Murray, see Section 2.3.1, are used respectively. Furthermore they consider a computational region in which there is a clear difference between the dermis and the epidermis, so that angiogenesis and wound closure can be simulated in separate regions. In Figure 2.9 the computational region is depicted.

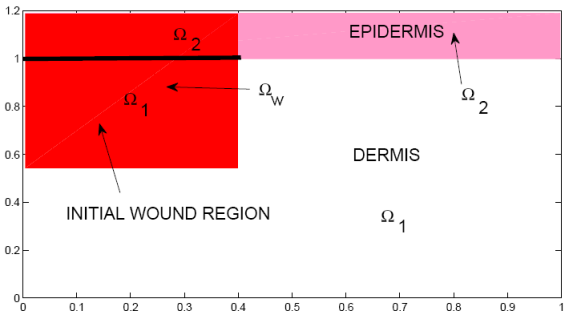

Figure 2.9: The geometry of the model with the dermis and the epidermis. This figure was taken, with permission, from [9].

The results in [9] show a clear sequence of the above mentioned stages of wound healing. Also, they partially overlap (although the amount of overlapping does depend on the choice of parameters) and thus influence one another, see Figures 2.10 and 2.11. For more details and results we refer to [9].

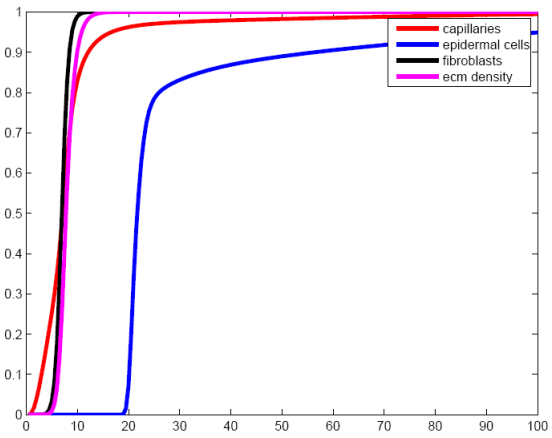

Figure 2.10: The concentration in the upper left part, see Figure 2.9, of the wound: capillary, ECM and fibroblast densities in the dermis, epidermal cell density in the epidermis. Here the capillary diffusity was taken $D_c = 0.01$ cm^2/s. This figure was taken, with permission, from [9].

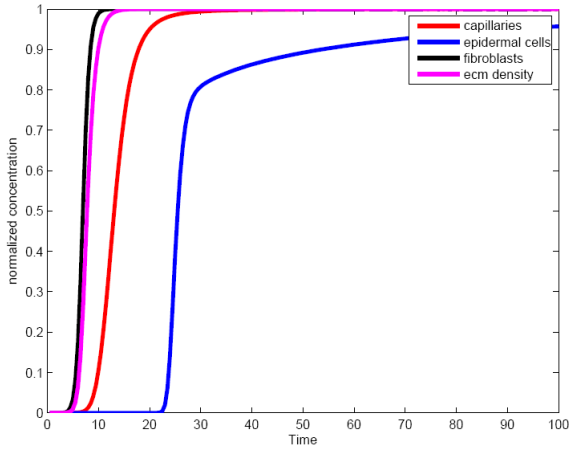

Figure 2.11: The concentration in the upper left part, see Figure 2.9, of the wound: capillary, ECM and fibroblast densities in the dermis, epidermal cell density in the epidermis. Here the capillary diffusity was taken $D_c = 0.001$ cm^2/s. This figure was taken, with permission, from [9].

Chapter 3

Some mathematical analysis on the visco-elastic equations

In this chapter we present some mathematical analysis on the visco-elastic problem. First, in Section 3.1, we construct analytic solutions for visco-elastic problems in $\mathbb{R}^1$. In Section 3.2 we investigate the stability of the visco-elastic problem.

This chapter is included to give some more insights on how the numerical solution should behave, i.e. their stability properties and steady state solution. These properties can be examined for the analytic solution. This analysis can be used to give an indication on what we may expect from the behaviour of the numerical solution computed for the wound contraction models.

3.1 Construction of analytic solutions for visco-elastic problems in $\mathbb{R}^1$

3.1.1 Homogeneous Dirichlet boundary conditions

The visco-elastic problem is used in Section 2.1 to model wound contraction. For $\Omega = [0,1] \subset \mathbb{R}^1$ with Dirichlet boundary conditions this problem is given by

$$\begin{cases} -(\mu_1+\mu_2)\frac{\partial^2}{\partial x^2}\left(\frac{\partial u}{\partial t}\right) - (\lambda+2\mu)\frac{\partial^2 u}{\partial x^2} + \gamma u = f(x), & \text{for } (x,t) \in \Omega \times \mathbb{R}^+, \\ u(0,t) = u(1,t) = 0, \\ u(x,0) = u^0(x). \end{cases} \tag{3.1}$$

Here we use the Lamé parameters λ and μ instead of E and ν for notational convenience. We use the eigenfunction expansion

$$u(x,t) = \sum_{k\geq 1} a_k(t)\sin(k\pi x) \tag{3.2}$$

and substitute this into equation (3.1). We may differentiate term by term since $u(x,t)$ and the eigenfunctions satisfy the same homogeneous boundary conditions, for more details see [12] page 116, and thus obtain the following differential equation for the a_k

$$(k\pi)^2(\mu_1+\mu_2)\frac{da_k}{dt} + ((\lambda+2\mu)(k\pi)^2+\gamma)a_k = f_k. \tag{3.3}$$

Here we have divided by $\sin(k\pi x)$, we may assume $\sin(k\pi x) \neq 0$, and the f_k are the coefficients of the Fourier sine series of $f(x)$, i.e.

$$f_k = 2\int_0^1 f(x)\sin(k\pi x)dx. \tag{3.4}$$

Note that f_k is a constant. The solution of (3.3) is then given by

$$a_k(t) = a_k^0 e^{\alpha_k t} + \frac{f_k}{(\lambda + 2\mu)(k\pi)^2 + \gamma}, \tag{3.5}$$

where α_k is given by

$$\alpha_k = -\left[\frac{\gamma}{(\mu_2 + \mu_2)(k\pi)^2} + \frac{\lambda + 2\mu}{\mu_1 + \mu_2}\right] \tag{3.6}$$

and a_k^0 can be obtained from the initial condition. We know that

$$u^0(x) = u(x, 0) = \sum_{k \geq 1} a_k(0) \sin(k\pi x). \tag{3.7}$$

Also we can write the initial solution as

$$u^0(x) = \sum_{k \geq 1} u_k^0 \sin(k\pi x), \tag{3.8}$$

where u_k^0 are the coefficients of the Fourier sine series of $u^0(x)$, i.e.

$$u_k^0 = 2 \int_0^1 u^0(x) \sin(k\pi x) dx. \tag{3.9}$$

So $a_k(0)$ must be equal to u_k^0 for all $k \geq 1$, i.e.

$$\frac{f_k}{(\lambda + 2\mu)(k\pi)^2 + \gamma} + a_k^0 = u_k^0.$$

This gives us as

$$a_k^0 = u_k^0 - \frac{f_k}{(\lambda + 2\mu)(k\pi)^2 + \gamma}. \tag{3.10}$$

Note that from (3.6) we can conclude that

$$\lim_{t \to \infty} a_k(t) = \frac{f_k}{(\lambda + 2\mu)(k\pi)^2 + \gamma}$$

and hence the steady state solution of problem (3.1) is given by

$$u^S(x) = \lim_{t \to \infty} u(x, t) = \sum_{k \geq 1} \frac{f_k}{(\lambda + 2\mu)(k\pi)^2 + \gamma} \sin(k\pi x). \tag{3.11}$$

Hence the solution of the linear visco-elastic problem on $[0, 1]$ with Dirichlet boundary conditions, problem (3.1), given by equation (3.2) converges to a steady state solution. This steady state solution is given by equation (3.11). In the next section we demonstrate a similar result, only now a homogenous Neumann boundary condition is assumed at $x = 1$.

3.1.2 Free boundary condition at $x = 0$

In this section we study the same visco-elastic problem as in Section 3.1.1, see equation (3.1), but now we assume a homogenous Neumann boundary condition at $x = 0$, i.e. $u_x(0) = 0$. We use the same concept to find a solution as in Section 3.1.1, only now the eigenfunction expansion is given by

$$u(x, t) = \sum_{k \geq 1} b_k(t) \cos(\frac{\pi}{2}(2k - 1)x). \tag{3.12}$$

Similar to a_k in Section 3.1.1, b_k then solves the differential equation

$$\frac{\pi^2}{4}(2k-1)^2(\mu_1+\mu_2)\frac{db_k}{dt} + ((\lambda+2\mu)\frac{\pi^2}{4}(2k-1)^2+\gamma)b_k = f_k. \tag{3.13}$$

Here f_k are the coefficients of the Fourier cosine series of $f(x)$, i.e.

$$f_k = 2\int_0^1 f(x)\cos(\frac{\pi}{2}(2k-1)x)dx. \tag{3.14}$$

The solution of (3.13) is given by

$$b_k(t) = b_k^0 e^{-\alpha_k t} + \frac{f_k}{(\lambda+2\mu)\frac{\pi^2}{4}(2k-1)^2+\gamma}, \tag{3.15}$$

where α_k is given by

$$\alpha_k = -\left[\frac{\gamma}{(\mu_2+\mu_2)\frac{\pi^2}{4}(2k-1)^2} + \frac{\lambda+2\mu}{\mu_1+\mu_2}\right] \tag{3.16}$$

and b_k^0 can be obtained from the initial condition. We know that

$$u^0(x) = u(x,0) = \sum_{k\geq 1} b_k(0)\cos(\frac{\pi}{2}(2k-1)x). \tag{3.17}$$

Also we can write the initial solution as

$$u^0(x) = \sum_{k\geq 1} u_k^0\cos(\frac{\pi}{2}(2k-1)x), \tag{3.18}$$

where u_k^0 are the coefficients of the Fourier cosine series of $u^0(x)$, i.e.

$$u_k^0 = 2\int_0^1 u^0(x)\cos(\frac{\pi}{2}(2k-1)x)dx. \tag{3.19}$$

So $b_k(0)$ must be equal to u_k^0 for all $k \geq 1$, i.e.

$$\frac{f_k}{(\lambda+2\mu)\frac{\pi^2}{4}(2k-1)^2+\gamma} + b_k^0 = u_k^0.$$

This gives us as

$$b_k^0 = u_k^0 - \frac{f_k}{(\lambda+2\mu)\frac{\pi^2}{4}(2k-1)^2+\gamma}. \tag{3.20}$$

Note that from (3.16) we can conclude that

$$\lim_{t\to\infty} b_k(t) = \frac{f_k}{(\lambda+2\mu)\frac{\pi^2}{4}(2k-1)^2+\gamma}$$

and hence the steady state solution of problem (3.1) is given by

$$u^S(x) = \lim_{t\to\infty} u(x,t) = \sum_{k\geq 1}\frac{f_k}{(\lambda+2\mu)\frac{\pi^2}{4}(2k-1)^2+\gamma}\cos(\frac{\pi}{2}(2k-1)x). \tag{3.21}$$

Hence the solution of the linear visco-elastic problem on $[0,1]$ with a homogenous Dirichlet boundary condition at $x=0$ and a homogenous Neumann boundary condition at $x=1$, given by equation (3.12), converges to a steady state solution. This steady state solution is given by equation (3.21).

3.2 Stability analysis of the visco-elastic equations

In this section we consider the stability of the steady-state solution of the visco-elastic equation. Suppose that $\mathbf{u}(\mathbf{x}, t)$ satisfies the following problem,

$$\begin{cases} -\nabla \cdot \sigma &= \mathbf{f}(\mathbf{x}), & (\mathbf{x}, t) \in \Omega \times \mathbb{R}^+, \\ \mathbf{u} &= \mathbf{0}, & (\mathbf{x}, t) \in \partial\Omega_1 \times \mathbb{R}^+, \\ \sigma \cdot \mathbf{n} &= \mathbf{0}, & (\mathbf{x}, t) \in \partial\Omega_2 \times \mathbb{R}^+, \\ \mathbf{u} &= \mathbf{0}, & (\mathbf{x}, t) \in \Omega \times \{0\}. \end{cases} \tag{3.22}$$

Here Ω is a Lipschitz domain in $\mathbb{R}^d$, with boundary $\partial\Omega = \partial\Omega_1 \cup \partial\Omega_2$ with $\partial\Omega_1 \cap \partial\Omega_2 = \emptyset$. The stress tensor σ is given by

$$\sigma = \sigma_{\mathrm{E}} + \sigma_{\mathrm{V}}, \tag{3.23}$$

where

$$\sigma_{\mathrm{E}} = \sigma_{\mathrm{E}}(\mathbf{u}) = 2\mu\epsilon + \lambda(\nabla \cdot \mathbf{u})\mathbf{I}, \tag{3.24}$$

$$\sigma_{\mathrm{V}} = \sigma_{\mathrm{V}}(\mathbf{u}) = \mu_1\epsilon_t + \mu_2(\nabla \cdot \mathbf{u}_t)\mathbf{I}. \tag{3.25}$$

Here $\mathbf{I}$ denotes the indentity tensor and the strain is denoted by

$$\epsilon = \epsilon(\mathbf{u}) = \frac{1}{2}\left(\nabla\mathbf{u} + (\nabla\mathbf{u})^T\right). \tag{3.26}$$

Now let

$$a(\mathbf{u}, \phi) = \int_\Omega \sigma_{\mathbf{E}}(\mathbf{u}) : \epsilon(\phi) d\Omega \tag{3.27}$$

and

$$b(\mathbf{u}, \phi) = \int_\Omega (\mu_1\epsilon(\mathbf{u}) + \mu_2(\nabla \cdot \mathbf{u})\mathbf{I}) : \epsilon(\phi) d\Omega. \tag{3.28}$$

Furthermore we define the function space Σ by

$$\Sigma = \left\{\psi \in \mathrm{H}^1(\Omega) : \ \psi = 0 \text{ for } \mathbf{x} \in \partial\Omega_1\right\} \tag{3.29}$$

Then solving (3.22) is equivalent to finding $\mathbf{u}(\mathbf{x}, t) \in \mathrm{L}^2\left([0, T]; \Sigma\right)$, subject to $\mathbf{u}(\mathbf{x}, 0) = \mathbf{0}$, such that

$$b(\mathbf{u}_t, \phi) + a(\mathbf{u}, \phi) = (\phi, \mathbf{f}) \tag{3.30}$$

for all $\phi \in \Sigma^2$. To this extent we state the following result about the existence and uniqueness of the steady state solution, $\mathbf{u}^S(\mathbf{x})$, which is defined by

$$\begin{cases} -\nabla \cdot \sigma_{\mathrm{E}}(\mathbf{u}^S) &= \mathbf{f}(\mathbf{x}), & \mathbf{x} \in \Omega, \\ \mathbf{u}^S &= \mathbf{0}, & \mathbf{x} \in \partial\Omega_1, \\ \sigma_{\mathrm{E}} \cdot \mathbf{n} &= \mathbf{0}, & \mathbf{x} \in \partial\Omega_2. \end{cases} \tag{3.31}$$

Theorem 3.2.1. *Problem (3.31) has one and only one solution in* Σ^2 *if* $\mathbf{f}(\mathbf{x}) \in \mathrm{L}^2(\Omega)$.

Proof. The proof resides on demonstrating that there is a unique $\mathbf{u}^S \in \Sigma^2$ such that

$$a(\mathbf{u}^S, \phi) = (\phi, \mathbf{f}) \tag{3.32}$$

for all $\phi \in \Sigma^2$. Since $a(\mathbf{u}^S, \phi)$ represents a bilinear form, we will show that $a(\mathbf{u}^S, \phi)$ is a coercive bilinear form. The bilinearity properties can be demonstrated in a very trivial way. Also

$$\begin{aligned} \sigma(\mathbf{u}) : \epsilon(\phi) &= (2\mu\epsilon(\mathbf{u}) + \lambda(\nabla \cdot \mathbf{u})\mathbf{I}) : \epsilon(\phi) \\ &= 2\mu\epsilon(\mathbf{u}) : \epsilon(\phi) + \lambda(\nabla \cdot \mathbf{u})(\nabla \cdot \phi) \end{aligned} \tag{3.33}$$

and thus is $a(\mathbf{u}, \phi)$ symmetric (and hence bounded). If we let

$$|\epsilon(\mathbf{u})| = \sqrt{\epsilon(\mathbf{u}) : \epsilon(\mathbf{u})}, \tag{3.34}$$

we immediately see from (3.33) that

$$\sigma(\mathbf{u}) : \epsilon(\mathbf{u}) \geq 2\mu |\epsilon(\mathbf{u})|^2. \tag{3.35}$$

This implies that

$$a(\mathbf{u}, \mathbf{u}) \geq 2\mu \int_\Omega \epsilon(\mathbf{u}) : \epsilon(\mathbf{u}) d\Omega = 2\mu ||\epsilon(\mathbf{u})||^2. \tag{3.36}$$

Next we use Korn's inequality, valid if $\text{meas}(\partial\Omega_1) > 0$ (see Corollary 11.2.22 in [13]), which states that there is a constant $C > 0$

$$||\epsilon(\mathbf{u})||^2 \geq C \left(||\nabla \mathbf{u}||^2 + ||\mathbf{u}||^2 \right), \tag{3.37}$$

to show that

$$a(\mathbf{u}, \mathbf{u}) \geq 2\mu C \left(||\nabla \mathbf{u}||^2 + ||\mathbf{u}||^2 \right) \tag{3.38}$$

and thus that $a(\mathbf{u}, \phi)$ is a coercive bilinear form. Then, by Lax-Milgram's Lemma, it follows that problem (3.31) has one and only one solution in Σ^2. □

Next, we consider convergence, and hence stability, to this steady state solution.

Theorem 3.2.2. *The solution of problem (3.30) converges to the solution of problem (3.31) as $t \to \infty$ almost everywhere (a.e.) in Ω.*

Proof. Let $\mathbf{v}(\mathbf{x}, t) = \mathbf{u}(\mathbf{x}, t) - \mathbf{u}^S(\mathbf{x})$, then $\mathbf{v}$ solves

$$\begin{cases} b(\mathbf{v}_t, \phi) + a(\mathbf{v}, \phi) &= \mathbf{0}, \qquad (\mathbf{x}, t) \in \Omega \times \mathbb{R}^+, \\ \mathbf{v} &= \mathbf{0}, \qquad (\mathbf{x}, t) \in \Omega \times \{0\}. \end{cases} \tag{3.39}$$

Note that

$$b(\mathbf{v}_t, \mathbf{v}) = -a(\mathbf{v}, \mathbf{v}),$$

which can be rewritten as

$$\frac{1}{2} \frac{d}{dt} b(\mathbf{v}, \mathbf{v}) = -a(\mathbf{v}, \mathbf{v}). \tag{3.40}$$

Next we know that μ_1, μ_2, μ and λ are all positive and finite real numbers and thus it is possible to find $\alpha > 0$ and $\beta > 0$ such that

$$\begin{aligned} \beta\mu_1 &\leq 2\mu \leq \alpha\mu_1 \\ \beta\mu_2 &\leq \lambda \leq \alpha\mu_2. \end{aligned}$$

From the above we may conclude that there are $\alpha, \beta > 0$ such that

$$\beta(\mu_1 + \mu_2) \leq 2\mu + \lambda \leq \alpha(\mu_1 + \mu_2)$$

and hence

$$\alpha b(\mathbf{v}, \mathbf{v}) \leq a(\mathbf{v}, \mathbf{v}) \leq \beta b(\mathbf{v}, \mathbf{v}). \tag{3.41}$$

Using the above we can change equation (3.40) to, there exists an $\alpha \in \left[0, \frac{2\mu+\lambda}{\mu_1+\mu_2}\right]$ such that

$$\frac{1}{2} \frac{d}{dt} b(\mathbf{v}, \mathbf{v}) \leq -\alpha b(\mathbf{v}, \mathbf{v}) \tag{3.42}$$

with

$$b(\mathbf{v},\mathbf{v})|_{t=0} = b(\mathbf{u}^S,\mathbf{u}^S).$$

Next, application of Grönwall's Lemma gives

$$0 \leq b(\mathbf{v},\mathbf{v}) \leq b(\mathbf{u}^S,\mathbf{u}^S)e^{-2\alpha t}, \tag{3.43}$$

which in turn, using the Squeeze Theorem, implies

$$\lim_{t\to\infty} b(\mathbf{v},\mathbf{v}) = 0. \tag{3.44}$$

Now, from (3.41), we may conclude that

$$\lim_{t\to\infty} a(\mathbf{v},\mathbf{v}) = 0, \tag{3.45}$$

and from this we see, since $a(\mathbf{v},\mathbf{v})$ is coercive, that the H^1-norm tends to zero as $t \to \infty$, i.e.

$$\lim_{t\to\infty} \left(||\nabla\mathbf{v}||^2 + ||\mathbf{v}||^2\right) = 0.$$

The above implies that

$$\lim_{t\to\infty} \mathbf{v}(\mathbf{x},t) = 0 \quad \text{a.e. in } \Omega$$

and thus that

$$\lim_{t\to\infty} \mathbf{u}(\mathbf{x},t) = \mathbf{u}^S(\mathbf{x}) \quad \text{a.e. in } \Omega.$$

□

Chapter 4

A novel model on angiogenesis

In Section 2.2 we presented two currently available models on angiogenesis, the process of capillary formation. These two models each take a very different approach on how to model this process. Where the model due to Maggelakis, [4], focusses on the relation between a lack of oxygen and capillary growth, the model due to Gaffney et al., [5], attempts to model the migration of endothelial cells into the wound. Both models adress an important aspect of angiogenesis, but on the other hand both also miss an important aspect.

In this section we present a novel angiogenesis model based on the models of Maggelakis and Gaffney et al. In this model we attempt to unite the two approaches and thus create a model that covers both aspects of angiogenesis. We wish to do so, since both models adress an important aspect of angiogenesis. Combining these two aspects in one model we hope to create a more accurate model of the process of angiogenesis. As a basis we take the model of Gaffney et al. and build in the mechanism depicted in Figure 2.6. This assures that both the endothelial cell migration and the oxygen shortage aspects are covered in this novel angiogenesis model.

The model due to Gaffney et al. is given by (2.20) and (2.21), where the functions f and g are given by

$$\begin{aligned} f(u_{\text{tip}}, u_{\text{end}}) =& \lambda_2 u_{\text{tip}} - \lambda_3 u_{\text{tip}}^2 - \lambda_4 u_{\text{tip}} u_{\text{end}}, \\ g(u_{\text{tip}}, u_{\text{end}}) =& \lambda_6 a u_{\text{end}}(u_{\text{end}}^0 - u_{\text{end}}) + \lambda_6 \chi u_{\text{tip}} u_{\text{end}}(u_{\text{end}}^1 - u_{\text{end}}) \\ & + \lambda_5(\lambda_3 u_{\text{tip}}^2 + \lambda_4 u_{\text{tip}} u_{\text{end}}). \end{aligned}$$

To incorporate the effects of the macrophage derived growth factor (MDGF) concentration c_{md} on the growth of capillary tips and the proliferation of endothelial cells we assume that λ_2 and λ_6 are functions of c_{md}. These functions must be zero if there is no MDGF present and rise as the MDGF concentration rises. Furthermore the effects of additional MDGF must be lower if there is already a lot of MDGF present. Therefore we let

$$\begin{aligned} \lambda_2(c_{\text{md}}) &= \lambda_2^0 \frac{c_{\text{md}}}{c_{\text{md}} + \tau_{\text{tip}}}, \\ \lambda_6(c_{\text{md}}) &= \lambda_6^0 \frac{c_{\text{md}}}{c_{\text{md}} + \tau_{\text{end}}}, \end{aligned}$$

where τ_{tip} and τ_{end} qualify how respectively λ_2 and λ_6 depend on the MDGF concentration. The functions $\lambda_2(c_{\text{md}})$ and $\lambda_6(c_{\text{md}})$ are given in Figure 4.1 for $0 \leq c_{\text{md}} \leq 1$.

This settles the trigger mechanism that the MDGF concentration fullfills in the growth of new capillaries. The PDE for the MDGF concentration remains the same as it only responds to a lack of oxygen and thus is still given by (2.18). Also for the oxygen concentration not much

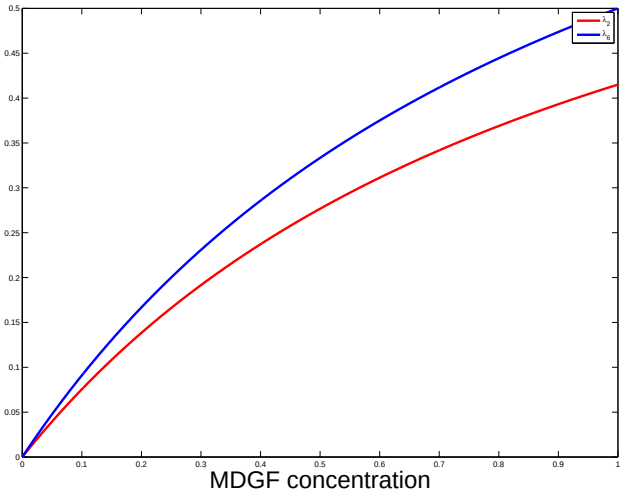

Figure 4.1: λ_2 and λ_6 as functions of c_{md}. Here we used $\tau_{\text{tip}} = \tau_{\text{end}} = 1$, $\lambda_2^0 = 0.83$ and $\lambda_6^0 = 1$.

changes, only now the oxygen is transported to the wound via both capillary tips and endothelial cells. Thus the last term in (2.17) changes to

$$\lambda_{13}\left(u_{\text{tip}} + \frac{\lambda_{\text{oxy}} u_\theta u_{\text{end}}}{\lambda_{13} u_{\text{end}}^0}\right).$$

With this last step we have created a novel angiogenesis model that incorporates both the effects of oxygen shortage and the migration of endothelial cells into the wound. To get a good overview of what the model looks like we give the PDEs that drive the model, i.e.

$$\frac{\partial u_{\text{oxy}}}{\partial t} = D_{\text{oxy}}\Delta u_{\text{oxy}} - \lambda_{\text{oxy}} u_{\text{oxy}} + \lambda_{13}\left(u_{\text{tip}} + \frac{\lambda_{\text{oxy}} u_\theta u_{\text{end}}}{\lambda_{13} u_{\text{end}}^0}\right), \tag{4.1}$$

$$\frac{\partial c_{\text{md}}}{\partial t} = D_{\text{md}}\Delta c_{\text{md}} - \lambda_{\text{md}} c_{\text{md}} + \lambda_{21} Q(u_{\text{oxy}}), \tag{4.2}$$

$$\frac{\partial u_{\text{tip}}}{\partial t} = \nabla\cdot\{D_1\nabla u_{\text{tip}} + D_2 u_{\text{tip}}\nabla u_{\text{end}}\} + f(u_{\text{tip}}, u_{\text{end}}), \tag{4.3}$$

$$\frac{\partial u_{\text{end}}}{\partial t} = \lambda_1\nabla\cdot\{D_1\nabla u_{\text{tip}} + D_2 u_{\text{tip}}\nabla u_{\text{end}}\} + g(u_{\text{tip}}, u_{\text{end}}), \tag{4.4}$$

where the functions f and g are given by

$$\begin{aligned} f(u_{\text{tip}}, u_{\text{end}}) =& \lambda_2^0 \frac{c_{\text{md}}}{c_{\text{md}} + \tau_{\text{tip}}} u_{\text{tip}} - \lambda_3 u_{\text{tip}}^2 - \lambda_4 u_{\text{tip}} u_{\text{end}}, \\ g(u_{\text{tip}}, u_{\text{end}}) =& \lambda_6^0 \frac{c_{\text{md}}}{c_{\text{md}} + \tau_{\text{end}}} \left(a u_{\text{end}}(u_{\text{end}}^0 - u_{\text{end}}) + \chi u_{\text{tip}} u_{\text{end}}(u_{\text{end}}^1 - u_{\text{end}})\right) \\ &+ \lambda_5(\lambda_3 u_{\text{tip}}^2 + \lambda_4 u_{\text{tip}} u_{\text{end}}). \end{aligned}$$

To show how this new model behaves we did some computations, from which some results can be seen in Figures 4.2 to 4.4. The computations have been done using numerical techniques described in Chapter 6. As a computational domain we use the unit square, i.e. $\Omega = \{\mathbf{x} = (x, y)|\ 0 \le x, y \le 1\}$, and the initial wound is given by $\Omega_w = \left\{\mathbf{x}|\ |\mathbf{x}| \le \frac{1}{2}\right\}$.

In Figure 4.2 we see the oxygen and MDGF concentration seven days after injury. The relation between a lack of oxygen and the production of the macrophage derived growth factor

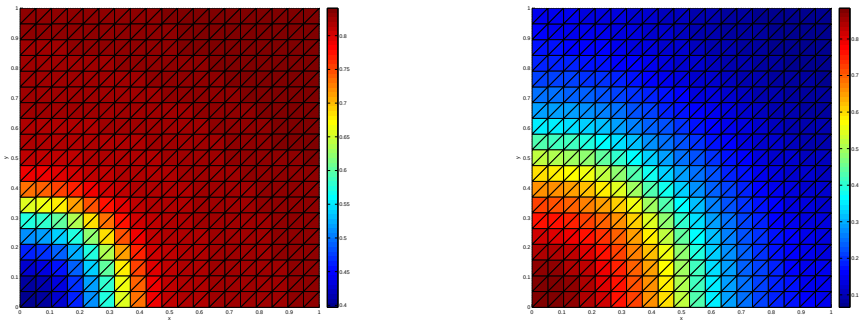

Figure 4.2: Normalized oxygen (left) and macrophage derived growth factor (right) concentration seven days after injury.

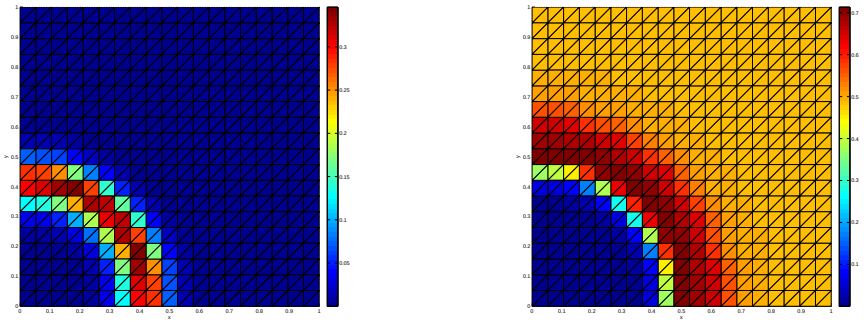

Figure 4.3: Normalized capillary tip concentration (left) and endothelial cell density (right) seven days after injury.

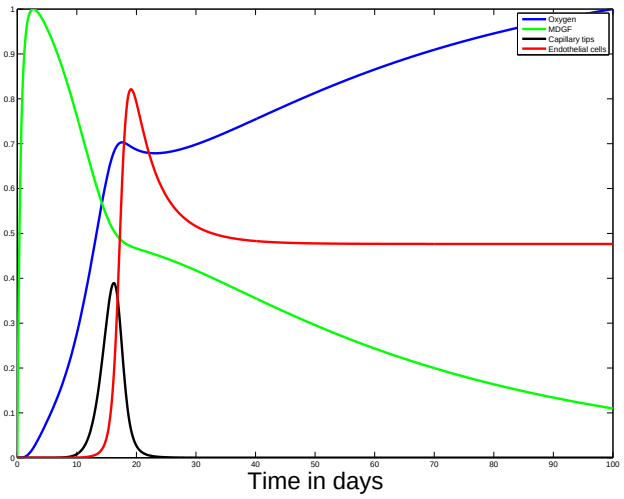

Figure 4.4: Normalized solutions furthest in the wound, at $\mathbf{x} = \mathbf{0}$, in time.

can clearly be seen. In areas where the oxygen concentration is low, i.e. inside the wound, the MDGF concentration is at its peak and vice versa. Also in Figure 4.4 we see that as the oxygen concentration rises the MDGF concentration drops at approximately the same rate.

Furthermore in Figure 4.3 we see a front of capillary tips, which slowly moves towards the center of the wound. Also the endothelial cell density is slighty elevated at the wound edge, since this is where the new capillaries are formed. This can also be seen in Figure 4.4, where the endothelial cell density first peaks and then drops again towards an equilibrium. The capillary tip concentration also peaks, but then drops to zero again. This is to be expected since eventually all capillary tips join together in the newly formed capillary network.

Chapter 5

Coupling between wound contraction and angiogenesis

For all three stages during the proliferative phase of wound healing mathematical models have been presented that attempt to describe the processes involved in these stages. These models only focus on one wound healing stage particularly and do not take into account the interactions between these stages. One example of interaction is the need of oxygen for the growth of cells and thus the dependency of the profileration terms on the oxygen concentration. But there are several more interactions that we can think of, including some that will not be taken into account here either.

In [9] an attempt is made to combine models of the three wound healing stages into one mathematical model. This model was discussed in Section 2.4. In this chapter we take the novel model on angiogenesis, presented in Chapter 4, and make an attempt to couple it with the wound contraction model due to Javierre given in Section 2.1.3. We will investigate both the influence of the oxygen concentration on the wound contraction mechanism and the influence of the fibroblast concentration on capillary growth. Furthermore the displacement of the extracellular matrix (ECM) will also effect the angiogenesis process, this will also be taken into account. For now we will not consider wound closure.

In the wound contraction stage several processes require energy to work. The growth of new tissue consumes energy as cells divide and form new cells, i.e. mitosis. Also the active movement of the fibroblasts requires energy since the cells crawl over each other, so to speak. This energy needed for wound contraction comes primarly from the food we eat, but oxygen is needed to put the energy to use, i.e. the cells require oxygen to get the most out of the energy. This means that the oxygen concentration is good indicator for the amount of energy that is available.

If we look at the partial differential equation (PDE) for the fibroblast concentration in the Javierre model,

$$\frac{\partial u_{\text{fib}}}{\partial t} + \nabla \cdot \left(\frac{\partial \mathbf{u}}{\partial t} u_{\text{fib}} - D_{\text{fib}} \nabla u_{\text{fib}} + \frac{a_{\text{fib}}}{(b_{\text{fib}} + c_{\text{ecm}})^2} u_{\text{fib}} \nabla c_{\text{ecm}} \right) =$$

$$\left(\lambda_{\text{fib}} + \frac{\lambda^0_{\text{fib}} c_{\text{ecm}}}{C_{1/2} + c_{\text{ecm}}} \right) u_{\text{fib}} \left(1 - \frac{u_{\text{fib}}}{K} \right) - \frac{p_{\text{cell}}(\theta)}{\tau_d + p_{\text{cell}}(\theta)} \frac{k_1 c_{\text{ecm}}}{C_k + c_{\text{ecm}}} u_{\text{fib}} + k_2 u_{\text{myo}} - d_{\text{fib}} u_{\text{fib}}, \quad (5.1)$$

the third term on the left hand side denotes the active convection and the first term on the right hand side respresents fibroblast proliferation. To incorporate the effects of the oxygen level on these two processes we replace these two terms with the following,

$$D_{\text{fib}} \frac{u_{\text{oxy}}}{\tau_{\text{oxy}} + u_{\text{oxy}}} \nabla u_{\text{fib}}$$

for the diffusion and

$$\frac{u_{\text{oxy}}}{\tau_{\text{oxy}} + u_{\text{oxy}}} \left(\lambda_{\text{fib}} + \frac{\lambda^0_{\text{fib}} c_{\text{ecm}}}{C_{1/2} + c_{\text{ecm}}} \right) u_{\text{fib}} \left(1 - \frac{u_{\text{fib}}}{K} \right)$$

for the proliferation of fibroblasts. The extra term in front, $\frac{u_{\text{oxy}}}{\tau_{\text{oxy}}+u_{\text{oxy}}}$, assures that if there is no oxygen present, i.e. no energy can be consumed, the two processes are stopped. When the tissue is saturated with oxygen the processes continue at their normal rate (the term then approaches one). Note that due to the PDE for the oxygen concentration the oxygenlevel will never rise to dangerous levels (the concentration moves towards an equilibrium), i.e. oxygen poisoning will never take place.

The proliferation of myofibroblasts also consumes energy and thus the same dependency on the oxygen concentration can be found in the PDE for the myofibroblasts. This concludes the influence of the oxygen level on wound contraction covered in this model.

The other way around wound contraction also effects the growth of new capillaries. First the displacement of the ECM causes passive convection of the variables of the angiogenesis model. This means that in each of the four equations an extra term is found that describes this passive convection, i.e.

$$\nabla \cdot \left(\frac{\partial \mathbf{u}}{\partial t} u_i \right),$$

where u_i denote the four variables of the novel angiogenesis model.

Furthermore the new capillaries need tissue to grow in. At first all tissue in the wound has been destroyed by the injury and so the capillaries can not grow. Gradually fibroblasts invade the wound and new tissue is formed. Only then can the recovery of the capillary network start. This is why it is reasonable to let the growth of capillaries depend on the fibroblast concentration.

The growth terms in (4.3) and (4.4) are given by

$$\lambda^0_2 \frac{c_{\text{md}}}{c_{\text{md}} + \tau_{\text{tip}}} u_{\text{tip}}$$

and

$$\lambda^0_6 \frac{c_{\text{md}}}{c_{\text{md}} + \tau_{\text{end}}} \left(a u_{\text{end}} (u^0_{\text{end}} - u_{\text{end}}) + \chi u_{\text{tip}} u_{\text{end}} (u^1_{\text{end}} - u_{\text{end}}) \right)$$

respectively. Similarly to how the oxygen concentration is coupled with the fibroblast PDE we couple the fibroblasts to the capillary tip and endothelial cell density PDEs. Therefor we introduce the factor

$$\frac{u_{\text{fib}}/u^0_{\text{fib}}}{\tau_{\text{fib}} + u_{\text{fib}}/u^0_{\text{fib}}}$$

in front of both production terms. This results in no capillary growth if there are no fibroblasts present, i.e. there is no tissue for them to grow in. As the fibroblast concentration rises the rate of capillary growth also rises towards its normal rate, since the term approaches one.

This concludes the coupling between the wound contraction model due to Javierre and the novel angiogenesis model covered in this thesis. Of course there are several other interaction between them. One can for instance think about the differentation from fibroblasts to myofibroblasts and back, which surely also consumes energy. This could be a subject for further study.

Next we present some results of the computation done on the coupled model. The simulations have been done using numerical techniques described in Chapter 6. The values of the parameters used can be found in Appendix A. We vary the diffusion speeds of the fibroblasts and the oxygen,

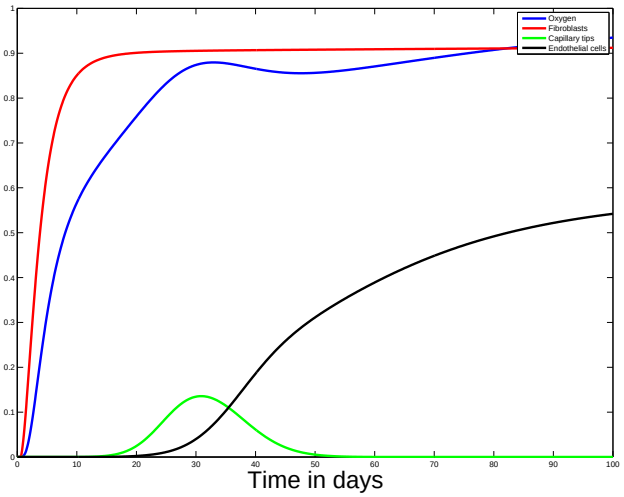

Figure 5.1: Normalized solutions furthest in the wound, at $\mathbf{x} = \mathbf{0}$, in time for $D_{\text{fib}} = 0.02$ and $D_{\text{oxy}} = 0.01$.

since we consider these to be of great importance (the problem seems to be diffusion dominated) and we would like to study the effect of these parameters on the solution.

In Figures 5.1 to 5.4 the results of the simulations can be found. The figures show the normalized solutions in time furthest in the wound, i.e. at $\mathbf{x} = \mathbf{0}$. The difference in diffusion speeds can clearly be seen in the graphs.

We see that with slow fibroblast diffusion the growth of capillaries start off at a later point in time. This is to be expected since the fibroblasts provide the tissue in which the capillaries can grow. The growth of the capillaries does follow a similar course. First the capillary tips find their way to the center of the wound and after that the capillary network is restored.

With a lower oxygen diffusion coefficient the oxygen reaches the center of the wound much later. Also the fibroblast concentration is effected. In Figure 5.2 we even see the fibroblast concentration drop very fast after it had risen due to fibroblasts diffusion. This shows the effect of the coupling. The oxygen concentration is still too low to provide enough energy for proliferation (growth of new cells) and so the fibroblasts concentration that grew due to diffusion drops again due to death.

Also with slower oxygen diffusion, the oxygen concentration depends more on the growth of new capillaries. In Figures 5.2 and 5.4 we see that the oxygen concentration rises far slower than 5.1 and 5.3. The oxygen concentration grows due to capillaries transporting oxygen to the wound side and not primarly due to diffusion.

We see that the varying the diffusion speeds has a major effect on the solutions. This confirms our idea that the problem is diffusion dominated. Although the solutions follow similar patterns in all cases, the differences can also be seen clearly.

Furthermore the coupling between the two models can also be seen. Especially with low diffusion speeds we see that the fibroblast concentration clearly depends on the oxygen concentration. Also the growth of new capillaries starts off later than in the uncoupled model, see Chapter 4. This can also be explained by the coupling, since the growth of capillaries is now dependend of the fibroblast concentration. So the growth can not begin untill there is enough tissue available, i.e. the fibroblast concentration is non-zero.

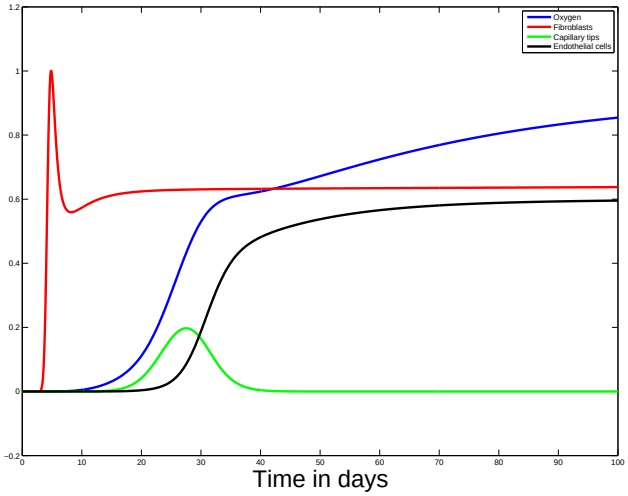

Figure 5.2: Normalized solutions furthest in the wound, at $\mathbf{x} = \mathbf{0}$, in time for $D_{\text{fib}} = 0.02$ and $D_{\text{oxy}} = 0.001$.

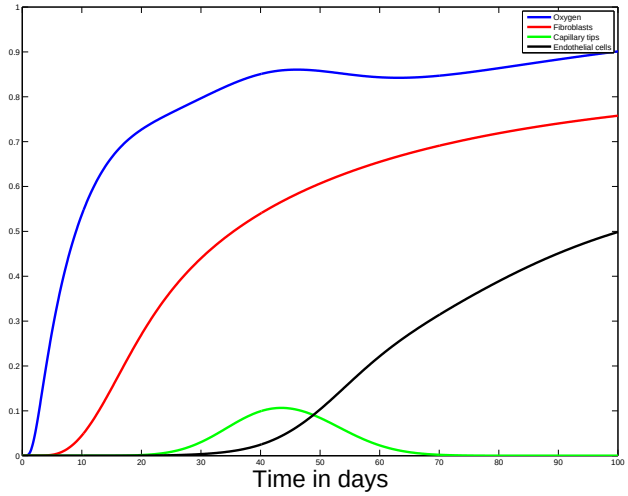

Figure 5.3: Normalized solutions furthest in the wound, at $\mathbf{x} = \mathbf{0}$, in time for $D_{\text{fib}} = 0.002$ and $D_{\text{oxy}} = 0.01$.

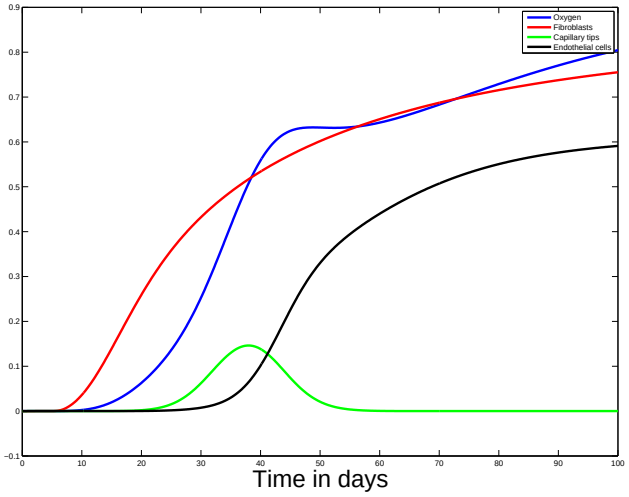

Figure 5.4: Normalized solutions furthest in the wound, at $\mathbf{x} = \mathbf{0}$, in time for $D_{\text{fib}} = 0.002$ and $D_{\text{oxy}} = 0.001$.

Chapter 6

Numerical methods

For several of the models mentioned in the previous chapters we presented computational results. In this chapter we give an overview on how these results were obtained, i.e. which numerical methods and techniques were used to obtain the solutions.

First, in Section 6.1, we show how we handle the space and time discretization of a nonlinear reaction-diffusion equation. We considers this type of equation as almost all partial differential equations (PDE) found in the wound healing models are of this type. Only the linear visco-elastic equations which we will discuss in Section 6.2, are not. This will also show how we take care of a system of coupled PDEs. All the programming to obtain the solution have been done in Matlab ©.

6.1 Reaction-diffusion equation

In this section we consider the nonlinear reaction-diffusion equation

$$\frac{\partial c}{\partial t} = D\Delta c + \lambda c(1-c) \quad \text{for } (\mathbf{x}, t) \in \Omega \times [0, T] \tag{6.1}$$

subject to

$$\begin{aligned} \frac{\partial c}{\partial n} &= 0 \quad \text{for } (\mathbf{x}, t) \in \partial\Omega \times [0, T], \\ c(0, \mathbf{x}) &= c_0(\mathbf{x}). \end{aligned}$$

Here D and λ are constants and n denotes the outward normal vector.

To discretize (6.1) in space we use the Finite Element Method (FEM). We multiply (6.1) by a testfunction η and integrate over the computational domain Ω to obtain

$$\int_\Omega \frac{\partial c}{\partial t}\eta d\Omega = \int_\Omega D\eta\Delta c + \lambda c(1-c)\eta d\Omega. \tag{6.2}$$

The testfunction η must be in the same space as c, i.e. η must be smooth and must satisfy the same boundary conditions as c. To the first term on the right hand side of (6.2) we apply the product rule for differentation and Gauss' Theorem. This gives us

$$\int_\Omega \frac{\partial c}{\partial t}\eta d\Omega = \int_\Omega -D\nabla\eta\cdot\nabla c + \lambda c(1-c)\eta d\Omega + D\int_{\partial\Omega}\eta\nabla c\cdot\mathbf{n}d\Gamma, \tag{6.3}$$

where the last term on the right hand side is equal to zero due to the boundary condition.

Next we use Galerkin's method and approximate c by

$$c^N = \sum_{j=1}^{N} c_j(t)\phi_j(\mathbf{x}). \tag{6.4}$$

The (basis) functions $\phi_j(\mathbf{x})$, $j = 1 \dots N$, must be in the same space as c, i.e. they must be sufficiently smooth and must satisfy the same boundary conditions. Furthermore we also want the testfunction η to be a linear combination of $\phi_j(\mathbf{x})$, i.e.

$$\eta = \sum_{j=1}^{N} b_j\phi_j(\mathbf{x}). \tag{6.5}$$

This choice is natural since the testfunction is in the same space as c. As η is chosen arbitrarily, we may assume that all b_j are equal to zero except for one, $b_i = 1$. Using this and substituting (6.4) and (6.5) into (6.3) we obtain

$$\frac{d}{dt}\sum_{j=1}^{N} c_j \int_\Omega \phi_i\phi_j d\Omega = -D\sum_{j=1}^{N} c_j \int_\Omega \nabla\phi_i \cdot \nabla\phi_j d\Omega + \lambda\sum_{j=1}^{N} c_j \int_\Omega (1-c)\phi_i\phi_j d\Omega \tag{6.6}$$

for $i = 1 \dots N$. Note that on the right hand side the term $1-c$ has not been approximated using Galerkin's method. This term is nonlinear and will lead to a nonlinear system of equations, which is not desirable. The term $1 - c$ will be evaluated at the previous timestep.

Note that (6.6) can be written in matrix-vector form,

$$M\frac{d\bar{c}}{dt} = S(c)\bar{c} + f, \tag{6.7}$$

where $\bar{c} = [c_1, c_2, \dots, c_N]^T$. We will omit the bar from now on and just write c. The (time) matrix M contains the integrals on the left hand side of (6.6),

$$M_{ij} = \int_\Omega \phi_i\phi_j d\Omega, \tag{6.8}$$

whereas $S(u)$, the mass matrix, contains the integrals on the right hand size

$$S(c)_{ij} = -D\int_\Omega \nabla\phi_i \cdot \nabla\phi_j d\Omega + \lambda\int_\Omega (1-c)\phi_i\phi_j d\Omega. \tag{6.9}$$

In this case $f = \mathbf{0}$, but normally it contains the terms in the original PDE that do not depend on c. Now we split the domain Ω up into (triangular) elements e_k and can construct the time and mass matrix using element matrices, see [10] for more details.

Let us denote the element time and mass matrix by M_e and $S_e(c)$ respectively. For the $\phi_j(\mathbf{x})$ we use the linear basisfunctions. The elements of M_e are then given, for $i, j = 1, \dots, 3$, using Newton-Cotes for a triangle with linear basisfunctions, by

$$\begin{aligned} M_e^{ij} &= \int_e \phi_i\phi_j de \\ &= \sum_{k=1}^{3} \phi_i(\mathbf{x}_k)\phi_j(\mathbf{x}_k)\int_e \phi_k de \\ &= \delta_{ij}\frac{|\Delta|}{6}. \end{aligned}$$

Here we have used local numbering, i.e. $\mathbf{x}_k$ denote the corners of the triangle and ϕ_k the corresponding basisfunctions that are not zero in the entire element. Furthermore Δ denotes the surface of the element. The elements of $S_e(c)$ are given by

$$S(c)_e^{ij} = -D\int_e \nabla\phi_i \cdot \nabla\phi_j de + \lambda \int_e (1-c)\phi_i\phi_j de,$$

for $i, j = 1, \ldots, 3$. In a similar way as done with the elements of M_e we can use Newton-Cotes to approximate the elements of $S_e(c)$ and find

$$S(c)_e^{ij} = -D\frac{|\Delta|}{2}(a_1^i a_1^j + a_2^i a_2^j) + \lambda(1 - c(\mathbf{x}_i))\frac{|\Delta|}{6}\delta_{ij}, \tag{6.10}$$

where a_l^k ($k = 1, \ldots, 3$, $l = 1, 2$) are derivatives of the linear basisfunctions and can be found in [10] at page 105. Furthermore note that the element mass matrix depends of the solution c due to the nonlinear term $1 - c$ in (6.1). This term wil be evaluated at the previous timestep as stated before.

This concludes the space discretization of (6.1). Both the time matrix M and the mass matrix $S(c)$ in (6.7) have been determined. Next step is to integrate (6.7) in time, more on this in Section 6.3.

6.2 Linear visco-elastic equations

To give an indication on how we handle the space discretization of a coupled system of partial differential equations we show in this section how we apply the methods presented in the previous section to the linear visco-elastic equations. The idea is similar, but some extra steps are needed.

The linear visco-elastic equations are given by

$$-\nabla \cdot \sigma = -s\rho\mathbf{u}, \tag{6.11}$$

where σ is the (second order) stress tensor and s is a constant. Furthermore we assume that there is no displacement on the boundary, i.e.

$$\mathbf{u} = \mathbf{0} \quad \text{for } (\mathbf{x}, t) \in \partial\Omega \times [0, T].$$

The stress tensor is given by

$$\sigma = \mu_1\frac{\partial\epsilon}{\partial t} + \mu_2\frac{\partial\theta}{\partial t}\mathbf{I} + \frac{E}{1+\nu}\left(\epsilon + \frac{\nu}{1-2\nu}\theta\mathbf{I}\right). \tag{6.12}$$

Here $\epsilon = \frac{1}{2}\left(\nabla\mathbf{u} + (\nabla\mathbf{u})^T\right)$ denotes the strain tensor and $\theta = \nabla \cdot \mathbf{u}$ the dilation. The other parameters are all constants.

As we did in Section 6.1 we multiply (6.11) by a testfunction $\eta = [\eta_1, \eta_2]^T$ and integrate over the computational domain Ω. The testfunction is a vectorfunction because there are two unknowns, namely u and v. Also η must be in the same space as $\mathbf{u}$, i.e. η is smooth and zero on $\partial\Omega$. We obtain

$$-\int_\Omega \eta\nabla \cdot \sigma d\Omega = -\int_\Omega \eta s\rho\mathbf{u} d\Omega. \tag{6.13}$$

Next we apply the product rule for differentation and Gauss' theorem to the left hand side to get

$$\int_\Omega \sigma \cdot \nabla\eta d\Omega = -\int_\Omega \eta s\rho\mathbf{u} d\Omega + \int_{\partial\Omega} \sigma \cdot \mathbf{n}\eta d\Gamma, \tag{6.14}$$

where the second integral on the right hand side is zero due to η being zero on the boundary.

Now note that the (second order) stress tensor σ can be written as

$$\sigma = \begin{pmatrix} \sigma_{11} & \sigma_{12} \\ \sigma_{21} & \sigma_{22} \end{pmatrix}$$

and thus that we can write (6.14) as two equations, i.e.

$$\int_\Omega \begin{bmatrix} \sigma_{11} \\ \sigma_{12} \end{bmatrix} \cdot \nabla \eta_1 d\Omega = -\int_\Omega s\rho u \eta_1 d\Omega, \tag{6.15}$$

$$\int_\Omega \begin{bmatrix} \sigma_{21} \\ \sigma_{22} \end{bmatrix} \cdot \nabla \eta_2 d\Omega = -\int_\Omega s\rho v \eta_2 d\Omega. \tag{6.16}$$

The elements of σ can be found from (6.12) and are given by

$$\begin{aligned}
\sigma_{11} =& \mu_1 \frac{\partial}{\partial t}\frac{\partial u}{\partial x} + \mu_2 \frac{\partial}{\partial t}\left(\frac{\partial u}{\partial x} + \frac{\partial v}{\partial y}\right) + \frac{E}{1+\nu}\frac{\partial u}{\partial x} + \frac{E}{1+\nu}\frac{\nu}{1-2\nu}\left(\frac{\partial u}{\partial x} + \frac{\partial v}{\partial y}\right), \\
\sigma_{12} = \sigma_{21} =& \frac{1}{2}\mu_1 \frac{\partial}{\partial t}\left(\frac{\partial u}{\partial x} + \frac{\partial v}{\partial y}\right) + \frac{1}{2}\frac{E}{1+\nu}\left(\frac{\partial u}{\partial y} + \frac{\partial v}{\partial x}\right), \\
\sigma_{22} =& \mu_1 \frac{\partial}{\partial t}\frac{\partial v}{\partial y} + \mu_2 \frac{\partial}{\partial t}\left(\frac{\partial u}{\partial x} + \frac{\partial v}{\partial y}\right) + \frac{E}{1+\nu}\frac{\partial v}{\partial y} + \frac{E}{1+\nu}\frac{\nu}{1-2\nu}\left(\frac{\partial u}{\partial x} + \frac{\partial v}{\partial y}\right).
\end{aligned}$$

Next we apply Galerkin's method and approximate u and v by

$$u^N = \sum_{j=1}^{N} u_j(t)\phi_j(\mathbf{x}) \tag{6.17}$$

and

$$v^N = \sum_{j=1}^{N} v_j(t)\phi_j(\mathbf{x}) \tag{6.18}$$

respectively. The (basis) functions $\phi_j(\mathbf{x})$, $j = 1 \ldots N$, must be in the same space as u and v, i.e. they must be sufficiently smooth and must satisfy the same boundary conditions. Furthermore we also want the testfunctions η_1 and η_2 to be a linear combination of $\phi_j(\mathbf{x})$, i.e.

$$\eta_1 = \sum_{j=1}^{N} b_j^1 \phi_j(\mathbf{x}), \quad \eta_2 = \sum_{j=1}^{N} b_j^2 \phi_j(\mathbf{x}). \tag{6.19}$$

Again we make a clever choice of the testfunctions, i.e. we let $b_j^k = 0$ for all j except for $b_i^k = 1$, where $k = 1, 2$. Now if we substitute (6.17), (6.18) and (6.19) in (6.15) and (6.16) we see that, as in Section 6.1, we can make a distinction between a time matrix M and a mass matrix S.

Next we split the domain Ω up into (triangular) elements e_k and can construct the time and mass matrix using element matrices, see [10] for more details. In this case there are two unknowns per nodal point and thus size of the element matrices is 6×6. But we can split up the element matrices into submatrices, as shown on page 128 of [10], i.e.

$$M_e = \begin{bmatrix} M_e^{uu} & M_e^{uv} \\ M_e^{vu} & M_e^{vv} \end{bmatrix}; \quad S_e = \begin{bmatrix} S_e^{uu} & S_e^{uv} \\ S_e^{vu} & S_e^{vv} \end{bmatrix}.$$

If we then use linear basis functions the elements of the submatrices of the element time matrix, for $i, j = 1, \ldots, 3$ are given by

$$
\begin{aligned}
M_e^{uu}(i,j) &= \frac{|\Delta|}{2}\left((\mu_1+\mu_2)a_i^1 a_j^1 + \frac{1}{2}\mu_1 a_i^2 a_j^2\right)\\
M_e^{uv}(i,j) &= \frac{|\Delta|}{2}\left(\mu_2 a_i^1 a_j^2 + \frac{1}{2}\mu_1 a_i^2 a_j^1\right)\\
M_e^{vu}(i,j) &= \frac{|\Delta|}{2}\left(\mu_2 a_i^2 a_j^1 + \frac{1}{2}\mu_1 a_i^1 a_j^2\right)\\
M_e^{vv}(i,j) &= \frac{|\Delta|}{2}\left((\mu_1+\mu_2)a_i^2 a_j^2 + \frac{1}{2}\mu_1 a_i^1 a_j^1\right).
\end{aligned}
$$

Here we used Newton-Cotes to approximate the integrals and a_l^k ($k = 1, \ldots, 3$, $l = 1, 2$) are derivatives of the linear basisfunctions and can be found in [10] at page 105. Note that the linear basis functions do not satisfy the same boundary conditions as u and v, i.e. they are not zero on the boundary. This can be circumvented, we show how in Section 6.3. In a similar way we can obtain the elements of the submatrices of the element mass matrix as

$$
\begin{aligned}
S_e^{uu}(i,j) &= -\frac{|\Delta|}{2}\left(\frac{E}{1+\nu}\left(1+\frac{\nu}{1-2\nu}\right)a_i^1 a_j^1 + \frac{1}{2}\frac{E}{1+\nu}a_i^2 a_j^2\right) - s\rho\frac{|\Delta|}{6}\delta_{ij}\\
S_e^{uv}(i,j) &= -\frac{|\Delta|}{2}\left(\frac{E}{1+\nu}\frac{\nu}{1-2\nu}a_i^1 a_j^2 + \frac{1}{2}\frac{E}{1+\nu}a_i^2 a_j^1\right)\\
S_e^{vu}(i,j) &= -\frac{|\Delta|}{2}\left(\frac{E}{1+\nu}\frac{\nu}{1-2\nu}a_i^2 a_j^1 + \frac{1}{2}\frac{E}{1+\nu}a_i^1 a_j^2\right)\\
S_e^{vv}(i,j) &= -\frac{|\Delta|}{2}\left(\frac{E}{1+\nu}\left(1+\frac{\nu}{1-2\nu}\right)a_i^2 a_j^2 + \frac{1}{2}\frac{E}{1+\nu}a_i^1 a_j^1\right) - s\rho\frac{|\Delta|}{6}\delta_{ij},
\end{aligned}
$$

for $i, j = 1, \ldots, 3$. Here δ_{ij} is the Kronecker delta.

This concludes the space discretization of (6.11). We are now left with a matrix-vector differential equation

$$
M\frac{d\mathbf{u}}{dt} = S\mathbf{u} \tag{6.20}
$$

where both the time matrix M and the mass matrix S in have been determined by the use of element matrices and their submatrices. The vector $\mathbf{u}$ contains the unknowns u_j and v_j, $j = 1, \ldots, N$. Next step is to integrate (6.20) in time, more on this in Section 6.3.

6.3 Time integration

In the previous sections we have shown how the (system of) partial differential equations are discritized in space. This leads in both cases to a coupled system of initial value problems of the form

$$
M\frac{d\mathbf{c}}{dt} = S(\mathbf{c})\mathbf{c}, \tag{6.21}
$$

accompanied by an initial condition $\mathbf{c}(0) = \mathbf{c}^0$. In (6.21) M and $S(\mathbf{c})$ are the time and mass matrix respectively.

To solve the solution $\mathbf{c}$ from (6.21) we must now integrate in time. We will denote the solution at time $t = t_m = m\Delta t$ as $\mathbf{c}^m$, where Δt is the timestep. Then if we use a Crank-Nicholson time integration scheme for (6.21) we obtain

$$
\left(M - \frac{1}{2}\Delta t S(\mathbf{c}^m)\right)\mathbf{c}^{m+1} = \left(M + \frac{1}{2}\Delta t S(\mathbf{c}^m)\right)\mathbf{c}^m. \tag{6.22}
$$

Note that the mass matrix S depends on the solution at the previous timestep. This is done to deal with nonlinearity in the partial differential equations as for example in (6.1). Normally the Crank-Nicholson scheme is second order accurate, but since we let the mass matrix S depend on the solution at the previous timestep we can only be sure that it is first order accurate. However in practice the accuracy will be somewhere between first and second order.

As stated in Section 6.2, if the variables satisfy Dirichlet boundary conditions we still have to do some work. We are now left with a matrix-vector equation of the form

$$A\mathbf{c} = b,$$

where $\mathbf{c}$ contains the unknowns at each timestep. Now suppose that c_j, for some $1 \leq j \leq N$, is located on the boundary $\partial\Omega$ and the solution there is subject to the Dirichlet boundary condition $c = c_{\mathrm{B}}$. We can then easily impose this boundary condition via the matrix vector equation. If we let $A_{j,j} = K$ and $b_j = Kc_{\mathrm{B}}$, where K is large compared to the other entries of A and b, then we automatically obtain the required boundary condition for c. This process is known as penalization.

After dealing with the essential boundary conditions we are left with solving the matrix-vector equation. This type of equation is easily solved in Matlab, especially as M and S are sparse matrices.

Chapter 7

Conclusions and future work

The proliferative phase of the wound healing process can be divided in three stages, i.e. wound contraction, angiogenesis and wound closure. For each separate stage there are currently several different models available. These are to some extent reasonable depictions of the real process.

In reality, of course, these separate stages overlap, they influence one another. Some of these influences have been investigated in this report with the coupling of two stages of the wound healing process, i.e. wound contraction and angiogenesis. The coupled model is diffusion dominated and thus the solution depends greatly on the choice of diffusion parameters. Investigating the solution's dependence on the model's parameters could be a topic for future research.

Also, in this report, a novel angiogenesis model has been proposed that combines the two already existing models of Maggelakis and Gaffney et al. It both incorporates the lack of oxygen mechanism that Maggelakis uses in his model and the capillary growth mechanism that is captured quite well in the model due to Gaffney et al. This novel model gives a reasonable depiction of how angiogenesis works quantitively, but also here the choice of parameters could be researched to also assure some level of qualitative correctness.

As said, a lot of work can still be done on the topic of wound healing. For future research we would recommend

1. Combination of the angiogenesis and wound contraction model with wound closure.
2. Modelling of the position of the basal membrane, which separates the dermis from the epidermis.
3. Investigating the choice of the model's parameters, to assure better qualitative correct models.

Appendix A

Parameter values for the coupled model

Parameter	Description	Value	Dimension
u_{fib}^0	Fibroblast density in healthy tissue	10^4	cells/cm^3
D_{fib}^0	Fibroblast diffusion rate	$2 \times 10^{-2}/2 \times 10^{-3}$	cm^2/day
a_{fib}	Determines, with b_{fib}, the maximal chemotaxis rate per unit GF conc.	4×10^{-10}	g/cm day
b_{fib}	GF conc. that produces 25% of the maximal chemotatic response	2×10^{-9}	g/cm^3
λ_{fib}	Fibroblast proliferation rate	0.832	day^{-1}
λ_{fib}^0	Maximal GF induced proliferation rate	0.3	day^{-1}
K	Determines the fibroblast equilibrium density	1×10^7	cells/cm^3
$C_{1/2}$	Half-maximal GF enhancement of fibroblasts proliferation	1×10^{-8}	g/cm^3
k_1	Maximal fibroblast to myofibroblast differentation rate	0.8	day^{-1}
k_2	Myofibroblast to fibroblast differentation rate	0.693	day^{-1}
C_k	Half-maximal GF enhancement of fibroblast to myofibroblast differentation	10^{-8}	g/cm^3
d_{fib}	Fibroblast death rate	0.831	day^{-1}
ε_{myo}	Myofibroblast to fibroblast logistic growth rate proportionality factor	0.5	-
d_{myo}	Myofibroblasts death rate	2.1×10^{-2}	day^{-1}
τ_{oxy}	Determines oxygen enhancement of (myo)fibroblasts proliferation	2×10^{-4}	

Table A.1: Parameters related to the fibroblast and myofibroblast equations.

Parameter	Description	Value	Dimension
ρ^0	Collagen concentration in healthy tissue	0.1	g/cm^3
ρ_{ini}	Initial collagen concentration in the wound	10^{-3}	g/cm^3
λ_ρ	Collagen production rate	7.59×10^{-10}	g^3/cm^6 cell day
λ_ρ^0	Maximal rate of GF induced collagen production	7.59×10^{-9}	g^3/cm^6 cell day
C_ρ	Half-maximal GF enhancement of collagen production	10^{-8}	g/cm^3
R_ρ	Half-maximal collagen enhancement of ECM deposition	0.3	g/cm^3
η_b	Myofibroblast to fibroblast collagen production rate proportionality factor	2	-
d_ρ	Collagen degradation rate per unit of cell density	7.59×10^{-8}	cm^3/cell day
η_d	Myofibroblast to fibroblast collagen degradation rate proportionality factor	2	-
c_{ecm}^0	Initial GF concentration in the wound	10^{-8}	g/cm^3
D_c	GF diffusion rate	5×10^{-2}	cm^2/day
k_c	GF production rate per unit of cell density	7.5×10^{-6}	cm^3/cell day
ζ	Myofibroblast to fibroblast chemical production rate proportionality factor	1	-
Γ	Half-maximal enhancement of net GF production	$\times 10^{-8}$	g/cm^3
d_c	GF decay rate	0.693	day^{-1}

Table A.2: Parameters related to the collagen and growth factor equations.

Parameter	Description	Value	Dimension
$p_{\max}$	Maximal cellular active stress per unit of ECM	10^{-4}	N g/cm2 cell
K_{pas}	Volumetric stiffness moduli of the passive components of the cell	2×10^{-5}	N g/cm2 cell
K_{act}	Volumetric stiffness moduli of the active filaments of the cell	1.852×10^{-5}	N g/cm2 cell
θ_1	Shortening strain of the contractile element	-0.6	-
θ_2	Lengthening strain of the contractile element	0.5	-
τ_d	Half-maximal mechanical enhancement fo fibroblast to myofibroblast differentation	10^{-5}	N g/cm2 cell
μ_1	Undamaged skin shear viscosity	200	N day/cm2
μ_2	Undamaged skin bluk viscosity	200	N day/cm2
E	Undamaged skin Young's modulus	33.4	N/cm2
ν	Undamaged skin Poisson's ratio	0.3	-
ξ	Myofibroblasts enhancement of traction per unit of fibroblasts density	10^{-3}	cm^3/cell
R_τ	Traction inhibition collagen density	5×10^{-4}	g/cm^3
s	Dermis tethering factor	5×10^2	N/cm g

Table A.3: Parameters related to the mechanical behaviour of cells and the ECM.

Parameter	Description	Value	Dimension
u^0_{oxy}	Oxygen concentration in healthy tissue	5	mg/cm^3
D_{oxy}	Oxygen diffusion rate	$10^{-2}/10^{-3}$	day^{-1}
λ_{oxy}	Oxygen decay rate	2×10^{-2}	day^{-1}
λ_{13}	Oxygen transport rate	1	day^{-1}
u_θ	Threshold value for macrophage derived GF	5	mg/cm^3
D_{md}	Macrophage derived GF diffusion rate	0.1	day^{-1}
λ_{md}	Macrophage derived GF decay rate	1	day^{-1}
λ_{21}	Macrophage derived GF production rate	10	day^{-1}
u^0_{tip}	Normalized initial capillary tip concentration in the small strip facing the wound	1	-
D_1	Capillary tip diffusion rate	3.5×10^{-4}	cm^2/day
u^0_{end}	Normalized endothelial cell density in healthy tissue	1	-
D_2	Endothelial cell diffusion rate	3.5×10^{-4}	cm^2/day
λ^0_2	Capillary tip growth rate	0.83	day^{-1}
τ_{tip}	Half-maximal macropahge derived GF enhancement of capillary tip growth	1	-
λ_3	Rate at which two capillary tips meet	0.83	day^{-1}
λ_4	Rate at which a capillary tip meets another capillary	0.85	day^{-1}
λ^0_6	Endothelial cell proliferation rate	1	day^{-1}
τ_{end}	Half-maximal macropahge derived GF enhancement of endothelial cell proliferation	1	-
a	Determines, with χ and u^1_{end}, the equilibrium endothelial cell density	0.25	-
χ	Determines, with a and u^1_{end}, the equilibrium endothelial cell density	0.3	-
u^1_{end}	Determines, with a and χ, the equilibrium endothelial cell density	10	-
λ_5	Capillary tip to capillary proportionality factor	0.25	-
τ_{fib}	Half-maximal fibroblast enhancement of capillary growth and endothelial cell proliferation	1	-

Table A.4: Parameters related to angiogenesis.

Bibliography

[1] V. Kumar, A. Abbas and N. Fausto: *Robbins and Cotran Pathologic Basis of Disease*, Philadelphia: Elsevier Saunders; 2005.

[2] J.D. Murray: *Mathematical Biology II: Spatial Models and Biomedical Applications*, New York: Springer-Verlag; 2004.

[3] L. Olsen, J.A. Sherratt and P.K. Maini: *A mechanochemical model for adult dermal wound closure and the permanence of contracted tissue displacement*, Journal of Theoretical Biology 1995; 177:113-128.

[4] S.A. Maggelakis: *A mathematical model for tissue replacement during epidermal wound healing*, Applied Mathematical Modelling 2003; 27:189-196.

[5] E.A. Gaffney, K. Pugh and P.K. Maini: *Investigating a simple model for cutaneous wound healing angiogenesis*, Journal of Theoretical Biology 2002; 45:337-374.

[6] J.A. Sherratt and J.D. Murray: *Mathematical analysis of a basic model for epidermal wound healing*, Journal of Theoretical Biology 1991; 29:389-404.

[7] J.A. Adam: *A simplified model of wound healing (with particular reference to the critical size deffect)*, Mathematical and Computer Modelling 1999; 30:23-32.

[8] F.J. Vermolen and E. Javierre: *A suite of continuum models for different aspects in wound healing*, In: Bioengineering research of chronic wounds, studies in mechanobiology, tissue engineering and biomaterials, New York: Springer-Verlag; 2009.

[9] F.J. Vermolen and E. Javierre: *Computer simulations from a finite-element model for wound contraction and closure*, Journal of Tissue Viability 2010; 19:43-53.

[10] J. van Kan, A. Segal and F.J. Vermolen: *Numerical Methods in Scientific Computing*, Delft: VSSD; 2005.

[11] E. Javierre, P. Moreo, M. Doblaré and J.M. García-Aznar: *Numerical modeling of a mechano-chemical theory for wound contraction analysis*, International Journal of Solids and Structures 2009; 46:3597-3606

[12] R. Habermann: *Applied partial differential equations with Fourier series and boundary value problems*, 4^{th} edition, London: Pearson Education; 2004.

[13] S.C. Brenner and L.R. Scott: *The mathematical theory of finite element methods*, 3^{rd} edition, New York: Springer; 2008.